

Quantitative T_2 Magnetic Resonance Imaging

Inauguraldissertation

zur Erlangung der Würde eines Doktors der Philosophie
vorgelegt der Philosophisch-Naturwissenschaftlichen
Fakultät der Universität Basel

von Hendrikus Joseph Alphons Crooijmans
aus Utrecht, die Niederlande

Basel, 2011

Genehmigt von der Philosophisch-Naturwissenschaftlichen Fakultät auf Antrag von

Prof. Dr. Klaus Scheffler
Dissertationsleiter

Prof. Dr. Sebastian Kozerke
Korreferent

Basel, den 21. Juni 2011

Prof. Dr. Martin Spiess
Dekan

Abstract

The exceptional soft tissue contrast of which MRI benefits, makes it an important tool for medical diagnosis. Not only the contrast itself, but also the possible quantification of relaxation times T_1 and T_2 causing this contrast is of interest. This quantification has proven to be clinically useful in the context of neurological diseases such as schizophrenia, autism, Parkinson's disease and many others.

The principle method used to quantify transverse relaxation time T_2 is the spin echo (SE) sequence which takes rather long. T_2 quantification for medical diagnosis is not often used because of this. A recently developed T_2 quantification method, driven equilibrium single pulse observation of T_2 (DESPOT2) offers the possibility of volumetric T_2 quantification within a clinical acceptable time with a resolution of less than 1 mm isotropic. The DESPOT2 method uses two balanced steady state free precession (bSSFP) acquisitions and prior knowledge of T_1 to determine T_2 .

The bSSFP acquisition on brain tissue is known to be magnetization transfer (MT) sensitive. Within this thesis' chapter 2, the effect of MT on the observed T_2 by DESPOT2 is investigated, and the outcome compared to the SE observation of T_2 . Within this chapter it is presented that MT reduces the observed T_2 and that this reduction can be avoided by the use of elongated excitation pulses.

The introduction of elongated RF excitation pulses introduces finite pulse effects: magnetization decay during part of the RF excitation pulse. Since the DESPOT2 method is based on a theory assuming instantaneous excitation, the observed T_2 calculation in this case contains a flaw which error size depends on the RF pulse duration. In chapter 3, the finite pulse effect on the DESPOT2 T_2 calculation is investigated and a correction for this effect is presented.

The DESPOT2 theory with incorporated finite pulse effect allows the observation of T_2 to be independent of the RF pulse duration.

Although it is now possible to acquire MT free bSSFP images and calculate the T_2 with the DESPOT2 method without the finite pulse effect manipulating the observed T_2 value, the DESPOT2 method still underestimates the T_2 compared to the T_2 observed by SE. In chapter 4 it is shown that this underestimation is caused by the microscopic complexity of brain tissue which is overlooked by the observation of a single T_2 . Within the limit of a single pool the two methods observe approximately identical T_2 values since the single pool model on which both methods are based is restored. In brain tissue, the pool fractions are not approaching this limit and therefore the T_2 observed by the two methods is different. Within the SE observation, T_2 does not depend on the echo spacing as is commonly thought; however, the time span over which the T_2 decay is sampled should be longer than the T_2 observed. The DESPOT2 observation depends strongly on the flip angles used; however, as long as both flip angles remain $\ll 90^\circ$ the T_2 observed is always lower than that observed by SE. Further, the difference between the two methods has shown to be depending stronger on the fractional pool sizes than on the exchange rates.

Although the MT effect within the bSSFP acquisitions can be avoided by elongated RF excitation pulses and the thereby introduced finite pulse effects corrected within the DESPOT2 T_2 calculation, the DESPOT2 method still overlooks the microscopic complexity of brain tissue. Because of this, an underestimation of T_2 compared to SE T_2 observations occurs, of which the amount depends on the fractional pool sizes and the exchange rates.

Contents

ABSTRACT	7
PUBLICATIONS ARISING FROM THIS THESIS	17
Journal Papers	17
Conference Abstracts	17

1

INTRODUCTION TO T_2 QUANTIFICATION	21
INTRODUCTION	23
SEQUENCES	24
Spin Echo	24
Spoiled Gradient Echo	25
Balanced steady state free precession	25
QUANTIFICATION	27
Spin Echo Based T_2 Quantification	27
Spoiled Gradient Echo & Balanced Steady State Free Precession Based T_2 Quantification	27
INFLUENCES	29
Magnetisation Transfer	29
Finite Pulse Effect	30
Multiple T_1 and T_2 combinations	32
Other mechanisms	33
AIM OF THIS THESIS	34
OUTLINE OF THE THESIS	35
REFERENCES	37

2

INFLUENCE OF MT EFFECTS ON T_2 QUANTIFICATION WITH 3D BALANCED STEADY-STATE FREE PRECESSION IMAGING	45
INTRODUCTION	47
MATERIALS AND METHODS	48
Numerical Simulations	48
Experiments	48
RESULTS	50
Numerical Simulations	50
Experiments	51
DISCUSSION	54
CONCLUSIONS	55
REFERENCES	57

3

FINITE RF PULSE CORRECTION ON DESPOT2	61
INTRODUCTION	63
METHODS	64
DESPOT2 with Finite RF Pulses	64
Two-Pool Bloch Simulation	64
Single-Pool Bloch Simulation	65
Measurements	65
RESULTS	66
Finite Difference Simulations	66
Measurements	67
DISCUSSION AND CONCLUSIONS	69
ACKNOWLEDGMENTS	70
REFERENCES	71

4

SINGLE T_2 ACQUISITIONS ON A MULTI-T_2 SYSTEM	75
INTRODUCTION	77
METHODS	78
Modified Bloch equations	78
Signal intensity simulations and T_2 calculations	78
Measurements	79
RESULTS	80
Simulations	80
Measurements	80
DISCUSSION AND CONCLUSION	83
ACKNOWLEDGEMENTS	84
REFERENCES	85

5

SUMMARY AND OUTLOOK	89
SUMMARY	91
OUTLOOK	93
REFERENCES	95

6

ACKNOWLEDGEMENT

101

7

LIST OF PUBLICATIONS AND CURRICULUM VITAE

107

LIST OF PUBLICATIONS

109

Journal Publications

109

Conference Abstracts

109

CURRICULUM VITAE

III

Personal Data

III

Education

III

Publications Arising From This Thesis

Journal Papers

H.J.A. Crooijmans, M. Gloor, O. Bieri and K. Scheffler. Influence of MT effects on T_2 quantification with 3D balanced steady-state free precession imaging. *Magn Reson Med.* 65(1):195-201, 2010

H.J.A. Crooijmans, K. Scheffler and O. Bieri. Finite RF pulse correction on DESPOT2. *Magn Reson Med*, 65(3):858-862, 2010

Conference Abstracts

H.J.A. Crooijmans and K. Scheffler. TR/T_2 dependency of variable flip angle T_1 measurements, a simulation. *Proceedings of the 25th annual meeting of ESMRMB*, Valencia, Spain, October 2-4 2008

H.J.A. Crooijmans, K. Scheffler and O. Bieri. Effect of magnetization transfer on rapid T_2 estimation with phase-cycled variable nutation SSFP. *Proceedings of the 17th scientific meeting & exhibition of ISMRM*, Honolulu, USA, April 18-24 2009

H.J.A. Crooijmans, K. Scheffler and O. Bieri. The influence of finite long pulse correction on DESPOT2. *Proceedings of the ISMRM-ESMRMB Joint Annual Meeting*, Stockholm, Sweden, May 1-7 2010

H.J.A. Crooijmans, M. Gloor, K. Scheffler and O. Bieri. Single pool assumption in SE and DESPOT2 T_2 quantifications on multi- T_2 probes. *Proceedings of the 28th annual scientific meeting of ESMRMB*, Leipzig, Germany, October 6-8 2011

1

Introduction to T_2 Quantification

Absolute relaxation time determination is clinically useful in a range of neurological diseases, in flow perfusion studies and contrast agent studies. Within the introduction, an overview of the quantification techniques used in this thesis is given, starting by the sequences they are based on (spin echo, spoiled gradient echo, and balanced SSFP) leading to the actual quantification of the transverse magnetization. Quantification can be done by sampling the decay curve using spin echo acquisitions, or combining two spoiled gradient echo acquisitions and two balanced SSFP acquisitions for T_1 and T_2 quantification by DESPOT1 and DESPOT2.

After this introduction, three mechanisms influencing the signal acquired by a balanced SSFP sequence are explained: the magnetization transfer effect, the finite pulse effect, and the exchange between two measurable components. Magnetization transfer can reduce the obtained balanced SSFP signal and thereby affect the outcome of DESPOT2. Long RF pulse durations reduce the magnetization transfer effect, however, this affects the decay time of transverse component of the magnetization (finite pulse effect). Last but not least, the exchange between two compartments of measurable T_2 can also exchange magnetization. In this case a coupled two compartment is measured, which might affect the outcome of a single T_2 quantification. Therefore, these three mechanisms are introduced here, and their effect on the quantification methods is investigated and described later in this work.

INTRODUCTION

The contrast in magnetic resonance imaging (MRI) is caused by variations in proton density and relaxation times. However, MRI contrast can also originate from perfusion, diffusion, flow, oxygenation and magnetization transfer. MRI is thus a multi-parametric technique, of which the obtained contrast depends on the chosen acquisition method (pulse sequence) and its characteristic parameter settings. In conventional MRI, the contrast is caused by a variation in proton density and relaxation times. Both longitudinal and transversal magnetization components in homogeneous samples relax mono-exponentially to their thermal equilibrium state with characteristic decay times T_1 and T_2 . However, although the sample might be identical, two different measurements with identical sequences can result in different contrast in the image due to different sequence parameter settings or setup differences as well as differences between scanners when performed on separate scanners. This can be overcome by calculating the actual decay time of the sample rather than acquiring only an image with contrast depending on this decay time. For clinical diagnosis, a decay time weighted image might already give the desired information and is therefore preferred above a quantification map because of its shorter acquisition and reconstruction time. However, when interested in the properties of a specific tissue over time, quantification (for example of T_2) might be preferred since this does not depend on sequence parameter settings or setup changes, nor on the scanner, but solely on the quantified parameter.

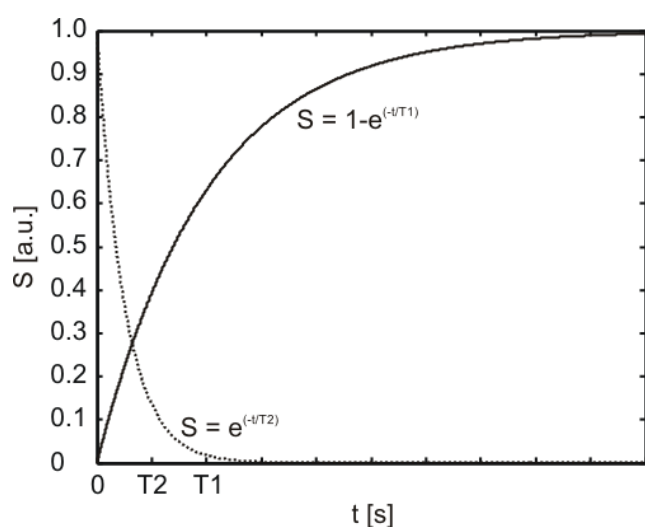


Figure 1. Signal intensity as a function of time: the longitudinal magnetization (line) builds up to the thermal equilibrium; the transverse magnetization (dotted line) decays to zero.

Absolute measurements of the relaxation times T_1 and T_2 is clinically useful: in the context of neurological disease variations in T_1 and T_2 have been demonstrated within specific brain regions within autism (1), schizophrenia (2), epilepsy (3), Parkinson's (4,5) and multiple sclerosis (6); in areas such as in-flow perfusion studies (7) and dynamic contrast agent studies (8).

The most basic quantification method for T_2 is the sampling of the T_2 decay curve (Fig. 1). The disadvantage of this approach is that it takes rather long to acquire a sufficient amount of data points for accurate estimation of T_2 . Therefore, the quest for a faster T_2 acquisition method has continued over the years. This has led to a faster variant of the spin-echo approach: the multi-echo spin-echo sequence (e.g. the Carr-Purcell sequence developed in 1954 (9) or the Carr-Purcell-Meiboom-Gill sequence developed in 1958 (10)). This sequence acquires multiple echoes during one single TR , reducing the total acquisition time.

Besides these SE based quantification techniques, T_2 quantification methods based on different sequences have been developed. Some techniques use preparation pulses such as T_2 (11) or Carr-Purcell prepared Snapshot FLASH (12) as well as the inversion recovery bSSFP (13) T_2 quantifications. Other techniques are based on partially spoiled SSFP (14) or balanced SSFP sequences (15).

Recently, a fast approach (the last of the above mentioned methods) has been developed that allows for the acquisition of both T_1 and T_2 (15). These methods, known as the driven equilibrium single pulse observant of T_1 and T_2 (DESPOT1 and DESPOT2), are based on radio frequency (RF) spoiled gradient echo (SPGR) and balanced steady-state free precession (bSSFP) acquisitions. Each DESPOT method uses only two acquisitions of sequences faster than the spin-echo sequence to calculate T_1 or T_2 . For the acquisition of T_2 , it uses two bSSFP acquisitions and prior knowledge of T_1 . Next to the above described methods, other methods have been developed; however, this thesis focuses on the DESPOT2 method, with the SE approach as a reference method since this method is still considered to be the golden standard.

This chapter of the thesis will introduce the used sequences, T_2 quantification methods as well as the investigated mechanisms that can influence the methods used in this thesis. It provides the information that might be desired to understand the succeeding work presented. The chapter will end with the aim and outline of the thesis.

SEQUENCES

Spin Echo

The spin echo sequence is the most common sequence and is based on the detection of a spin echo. It uses a 90° RF pulse to excite the magnetization (tilt it from along the longitudinal z-axis into the transverse xy-plane) and one or more 180° refocusing pulses to refocus the spins and make them create signal echoes, called spin echoes (Fig 2 shows the SE sequence timing diagram) (16,17). In case only one refocusing pulse is applied per TR , the sequence is called a single echo spin echo (SE) sequence. As soon as more echoes are acquired within a single TR , the sequence is called a multi echo spin echo (mSE) sequence.

is applied. The mSE sequence does not have this drawback, since it is capable of acquiring multiple echoes within one TR . Nevertheless, there is another drawback that occurs in the mSE acquisition: stimulated echoes.

Stimulated echoes can be produced by any RF pulse other than an ideal 180° RF pulse. A stimulated echo is an echo produced by three succeeding RF pulses: an excitation pulse, followed by two other RF pulses (e.g., α - β - β). The stimulated echo occurs after the third pulse, at a time equal to the time between the first two pulses. Within the mSE experiment, ideal 180° pulses are assumed; however, this can never be realized in practice. The spin-echoes in a mSE sequence are equally spaced, leading to simultaneously occurring spin-echoes

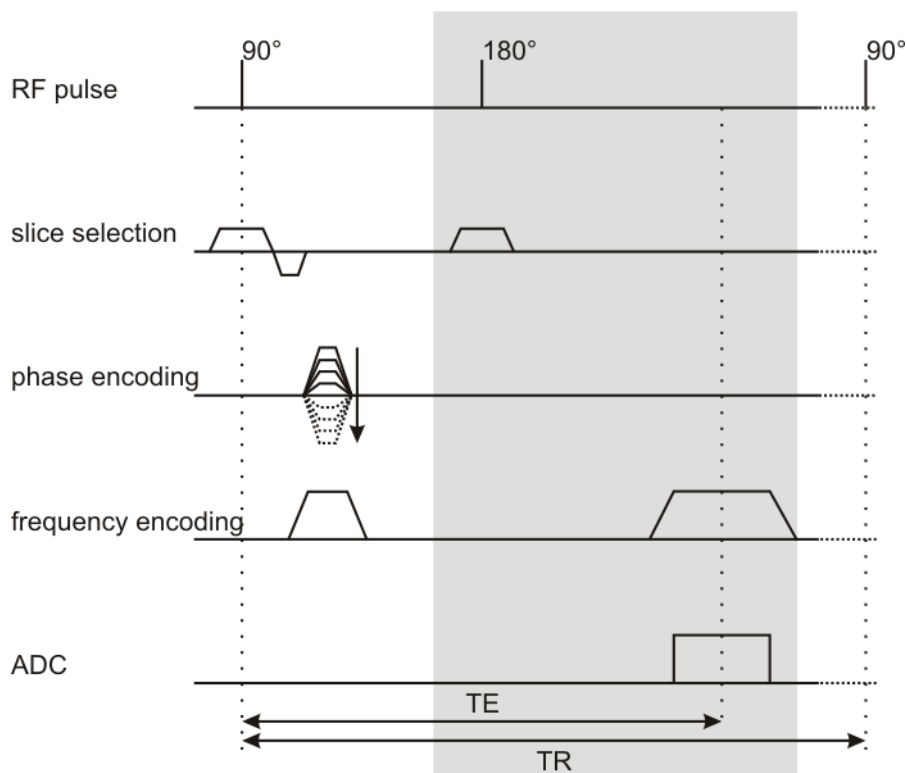


Figure 2. Sequence timing diagram of a spin echo sequence. The parts in gray can be repeated to turn the spin echo sequence into a multi-echo spin echo sequence.

The SE sequence can have proton density, T_1 and T_2 weighting depending on the choice of TR and TE :

- short TE and long TR : proton density weighted image
- short TE and short TR : T_1 weighted image
- long TE and long TR : T_2 weighted image

The main drawback of the SE sequence is its long acquisition time caused by the need to let the magnetization relax back to or close to the thermal resting state before a new excitation pulse

and stimulated echoes for all echoes except the first (17). Although the example above only demonstrates a three-pulse experiment, it is arbitrary that for a higher number of β pulses, more stimulated echoes will occur. The stimulated echoes in a mSE experiment occur due to non-ideal 180° pulses. The non-ideal 180° pulse occurrence is due to slice profile effects (non-ideal slice profile) of the slice selective excitation and refocusing pulses as well as they can be caused by B_1 inhomogeneities.

Spoiled Gradient Echo

Gradient echo (GRE) sequences do not necessarily use a 90° excitation pulse, and the excitation pulse is called an alpha pulse (α), usually set between 0° and 90° (16,17). A (spoiled) gradient echo sequence does not use a 180° refocusing pulse as the SE sequence does: the spins are first dephased by a negatively pulsed gradient before they are rephased by a gradient with opposite polarity to generate the echo (Fig. 3). From the constraint of constant dephasing within TR (18), the phase encoding gradient has to be rewound prior to the next excitation. Within a spoiled gradient echo (SPGR) sequence, the transverse magnetization remaining after the

signal approximate the Ernst equation (22):

$$S_{SPGR} = M_0 \sin \alpha \frac{1 - e^{-TR/T_1}}{1 - e^{-TR/T_1} \cos \alpha} \quad [2]$$

where M_0 is the equilibrium magnetization, α the excitation pulse and t the time after the excitation pulse. The SPGR signal intensity is maximal when the alpha pulse is set to the Ernst angle ($\alpha_{Ernst} = \cos^{-1}(e^{-TR/T_1})$). The SPGR sequence can result in either PD or T_1 weighted images:

- $\alpha < \alpha_{Ernst}$: PD weighted images
- $\alpha > \alpha_{Ernst}$: T_1 weighted images

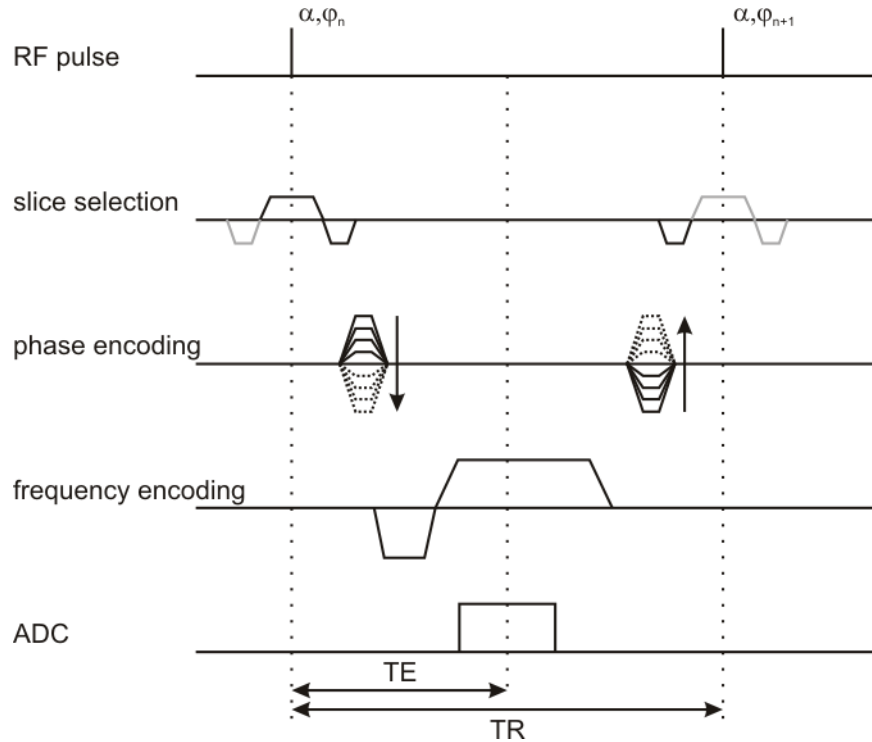


Figure 3. Sequence timing diagram of the spoiled gradient echo (SPGR) sequence. The spoiler gradient in this example is implemented in frequency encoding direction.

readout gradient is destroyed by a spoiler gradient. The obtained signal intensity is a function of both T_1 and T_2 and the resulting image thus exhibits a mixed T_1 and T_2 contrast (19).

For approximate T_1 weighting, additional RF spoiling is desired. Therefore, the phase (φ) of the RF pulse is incremented from one pulse to the next in a specific way:

$$\varphi_n = \frac{n(n+1)}{2} \varphi_{inc} \quad [1]$$

where (depending on the manufacturer) φ_{inc} is 50° or 117° (19-21). These and other possible values of leading to sufficient RF spoiling make the SPGR

Balanced steady state free precession

Within a steady state free precession (SSFP) sequence, the TR is typically chosen to be less than T_2 ($TR < T_2$). In this situation, even the transverse magnetization does not relax back to zero, as it can within a SE sequence. Neither is there a spoiling gradient at the end of TR to spoil the remaining transverse magnetization. Under these circumstances, the signal just before to the next RF excitation pulse has both longitudinal and transverse components. Over a number of repetitions, a dynamic equilibrium or steady state is build up. In the steady state, the magnetization is periodic over TR . Long before fast sequences such as the SSFP sequences were available; the theoretical treatment

of the steady state was described by Carr in 1958 (23), and by Freeman and Hill in 1971 (24), and by Hinshaw in 1976 (25).

For non-balanced SSFP sequences, the transverse magnetization at just before the next RF excitation pulse ($t = TR$) is dephased due to a dephasing gradient before or after the readout, and it contributes to the signal evolution. The transverse magnetization before the RF pulse is named the ECHO, the transverse magnetization after the RF pulse is called the FID. The dephasing moment of the readout gradient can be shaped to generate an echo from the ECHO or from the FID (16).

In balanced SSFP (bSSFP), the dephased magnetization is fully rephased by a reverse gradient pulse (Fig. 4), and the bSSFP sequence produces the highest signal amplitudes of all SSFP sequences. Great advantage of the bSSFP sequence is its flow compensated behavior: spins with constant flow in the slice- and readout-direction are not restrained from any reduced dephasing during TR . The bSSFP sequence is very sensitive to static field (B_0) inhomogeneities. Therefore, shimming prior to the bSSFP acquisition is favorable to homogenize the B_0 field to avoid off-resonance effects. Since the bSSFP also depends highly on gradient performance, bSSFP sequences have only been used in clinical routine for approximately 10 years.

Alternating RF pulses (i.e., RF phase increment of 180°) and centered echoes ($TE = TR/2$) are typically used in bSSFP acquisitions to yield steady

state signal (24,26). Although multiple forms of the SSFP signal equation are presented in literature (23,27-31), when the TR is also kept short ($TR < 10$ ms), the equation derived by Perkins and Wehrli (30) is most appropriate and denotes the signal directly after the RF pulse:

$$S_{SSFP} = M_0 \sin \alpha \cdot \frac{1 - e^{-TR/T_1}}{1 - e^{-TR/T_1} e^{-TR/T_2} - (e^{-TR/T_1} - e^{-TR/T_2}) \cos \alpha} \quad [3]$$

The above restriction of TR in general yields $TR \ll T_1, T_2$ and the signal can be shown to be proportional to $\sqrt{T_2/T_1}$ (17). Because of this, fluids and fat appear hyper intense in the bSSFP images compared to gray and white matter. The contrast between gray and white matter is only little, due to their comparable T_2/T_1 ratios.

The characteristic parameters in a bSSFP acquisition are:

- the repetition time TR
- the flip angle α

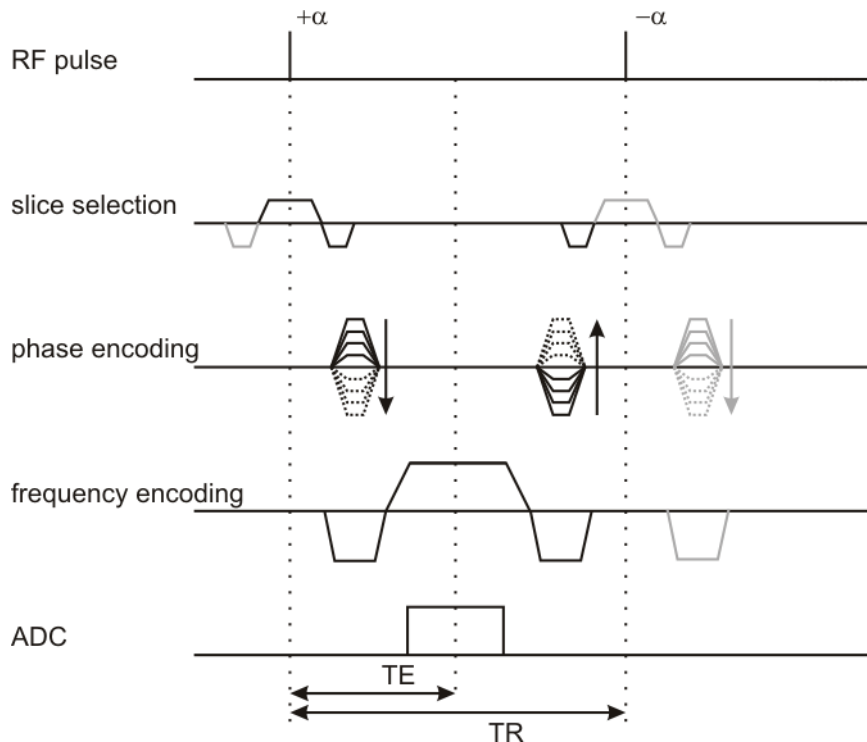


Figure 4. Sequence timing diagram of the balanced steady state free precession (bSSFP) sequence.

QUANTIFICATION

Spin Echo Based T_2 Quantification

The T_2 decay can be visualized by a series of SE acquisitions sampling the decay curve. Therefore, the SE acquisition has to be repeated for every sample point with its own unique TE to sample the signal decay at several points after the 90° excitation pulse. The T_2 is acquired by the fitting of a mono-exponential function (Eq. 4) through the signal intensities (S) at these sample points.

$$S = M_0 e^{-t/T_2} \quad [4]$$

M_0 is the equilibrium magnetization, t the time after the 90° excitation pulse and T_2 the desired parameter to obtain. The characteristic parameters of the SE sequences in T_2 quantification are:

- the echo times TE or the placing of the sample points
- the number of echoes or sample points
- the time span of the decay curve sampling

The SE sequence has to have a long TR to ensure (almost) complete relaxation to the thermal steady state within TR . Due to this requirement on TR , the SE based T_2 quantification method is rather time consuming. This can be overcome by the use of the mSE sequence rather than the SE sequence. However, the mSE sequence suffers from non-ideal slice profiles and stimulated echoes. The influence of the non-ideal slice profile can be reduced by application of larger echo spacing by which the resulting underestimation of T_2 becomes negligible. However, too large values for TE lead to severe SNR reduction which is not wise. Since the first acquired echo is hypo-intense due to a possible lack of stimulated echo contributions (32), it is often discarded from the analysis. However, the stimulated echoes can also be compensated for, as has been proposed recently in (32), which allows inclusion of all echoes into the analysis. Overall, the SE approach is still considered the 'golden standard' in T_2 quantification because it is least sensitive to or does not suffer at all from the mentioned effects.

Spoiled Gradient Echo & Balanced Steady State Free Precession Based T_2 Quantification

A relatively new quantification approach determines both T_1 and T_2 . This technique does not sample the decay curve like the SE based T_2 quantification: it uses the SPGR signal curve depending on T_1 which can be easily linearized for T_1 quanti-

fication; and the bSSFP signal curve depending on both T_1 and T_2 , also cast in the linear form allowing for T_2 quantification assuming prior knowledge of T_1 . These methods for T_1 and T_2 quantification are known as the driven-equilibrium single-pulse observation of T_1 and T_2 , DESPOT1 and DESPOT2 (15).

DESPOT1 theory

The SPGR signal intensity is a function of the longitudinal relaxation time T_1 , the repetition time TR , the flip angle α , and a factor which is proportional to the equilibrium longitudinal magnetization M_0 (Eq. 5). A T_1 characterized curve is generated when incrementally increasing α while holding TR constant. These data can be presented in a linear form ($Y = mX + b$), as demonstrated in (33), and results in:

$$\frac{S_{SPGR}}{\sin \alpha} = e^{-TR/T_1} \frac{S_{SPGR}}{\tan \alpha} + M_0 (1 - e^{-TR/T_1}) \quad [5]$$

From this, the slope m can be estimated by means of linear regression, allowing T_1 to be extracted:

$$T_1 = -TR / \ln(m) \quad [6]$$

The method has been originally introduced in 1974 (34) and parameters influencing the DESPOT1 method have been investigated by others (35-38). Wang et al. (35) reported that the T_1 precision obtained using 10 flip angles can also be achieved by just two optimally chosen flip angles. This leads in a five-fold reduction of scan time. To determine the optimal flip angles to reach this precision, Deoni et al. (15) have obtained an analytical solution:

$$\alpha = \cos^{-1} \left(\frac{f^2 e^{-TR/T_1} \pm (1 - e^{-2TR/T_1}) \sqrt{1 - f^2}}{1 - e^{-2TR/T_1} (1 - f^2)} \right) \quad [7]$$

Where f is the fractional signal defined as $f = S/S_0$. They have also shown that the T_1 precision is maximized when $f = 0.71$. Hereby, the flip angles for optimal T_1 precision at any given TR/T_1 combination can be determined.

DESPOT2 theory

The bSSFP signal intensity is a function of T_1 , T_2 , TR , α , and M_0 (Eq. 8). Data acquired with constant TR while incrementally increasing the flip angle α will be depending on T_1 as well as T_2 . This equation can also be rewritten to a linear form ($Y = mX + b$) and becomes:

$$\frac{S_{bSSFP}}{\sin \alpha} = \frac{e^{-TR/T_1} - e^{-TR/T_2}}{1 - e^{-TR/T_1} e^{-TR/T_2}} \frac{S_{bSSFP}}{\tan \alpha} + \dots \quad [8]$$

$$\frac{M_0 (1 - e^{-TR/T_1})}{1 - e^{-TR/T_1} e^{-TR/T_2}}$$

If T_1 is known, e.g. from a prior DESPOT1 acquisition, T_2 can be calculated from the slope m :

$$T_2 = -TR / \ln \left(\frac{m - e^{-TR/T_1}}{m e^{-TR/T_1} - 1} \right) \quad [9]$$

Since the signal intensity of the bSSFP sequence is depending on T_1 , T_2 , TR and α , the optimal flip angle calculation will depend on TR , T_1 and T_2 . Deoni et al. (15) have found an analytical solution for the determination of the flip angles desired for optimal T_2 precision (Eq. 10). The maximal T_2 precision is achieved for $f = 0.71$.

$$\alpha = \cos^{-1} \left(\frac{-B \pm \sqrt{B^2 - 4AC}}{2A} \right) \quad [10]$$

where:

$$A = -1 + 2e^{-TR/T_1} e^{-TR/T_2} - e^{-2TR/T_1} e^{-2TR/T_2} \dots$$

$$+ 2(e^{-TR/T_1} - e^{-TR/T_2}) \varphi - \dots \quad [11]$$

$$2e^{-TR/T_1} e^{-TR/T_2} (e^{-TR/T_1} - e^{-TR/T_2}) \varphi - \dots$$

$$(e^{-TR/T_1} - e^{-TR/T_2})^2 (1 - \varphi)^2 f^2$$

$$B = 2(e^{-TR/T_1} - e^{-TR/T_2}) \dots$$

$$(1 - e^{-TR/T_1} e^{-TR/T_2}) (1 - \varphi^2) f^2 \quad [12]$$

$C =$

$$(1 - e^{-TR/T_2} \varphi)^2 - (1 - \varphi^2) f^2 + \dots$$

$$e^{-2TR/T_1} \left(\frac{2e^{-TR/T_2} \varphi + \varphi^2 + e^{-2TR/T_2} \dots}{(1 - f^2 (1 - \varphi^2))} \right) - \dots \quad [13]$$

$$2e^{-TR/T_1} \left(\frac{\varphi + e^{-2TR/T_2} \varphi + e^{-TR/T_2} \dots}{(1 + \varphi^2 - f^2 (1 - \varphi^2))} \right)$$

$$\varphi = \frac{e^{-TR/T_1} - e^{-TR/T_2}}{1 - e^{-TR/T_1} e^{-TR/T_2}} \quad [14]$$

INFLUENCES

There are several mechanisms influencing the obtained signal of the used sequences. Although the SE sequence is hardly sensitive to any of the mentioned mechanisms below, the bSSFP sequence is rather highly sensitive.

Magnetisation Transfer

The interaction between free water protons and macromolecular protons forms the basis of the magnetization transfer (MT) effect. Next to these two proton sources, exchangeable protons in a hydration layer around the macromolecule play an important role in the MT process (39-41). There are two proposed pathways of MT between macromolecule and water:

- MT between non exchangeable protons and exchangeable protons of hydroxyl or amine groups (OH and NH, respectively) of the macromolecule by magnetic dipole-dipole interactions (Nuclear Overhauser Effect (NOE)). The intermediate proton exchanges the magnetization rapidly with the free water (Fig. 5).
- The hydration layer water protons take the role of the hydroxyl or amine groups, interacting with the non exchangeable protons of the macromolecule. Afterwards, they rapidly exchange magnetization with the free water (Fig. 5) (40,41).

MT between water and lipid membrane models has shown to be dependent on the sites with exchangeable hydroxyl and amino protons (42), and thus on the first of the above mentioned two pathways. The exchange rates of the amino and hydroxyl protons are sufficiently fast to not be rate limiting for the overall MT, and sufficiently slow for optimum dipole-dipole interactions with the non exchangeable protons of the macromolecule. Furthermore, the hydration layer water molecules are less effective in dipole-dipole transfer of magnetization (41).

The restricted protons of the macromolecule have very short decay times ($T_2 \approx 10 \mu\text{s}$) and can therefore not be detected with conventional proton MRI. The macromolecular spins however, exhibit a broader absorption lineshape than the free water protons. Therefore, the restricted protons can indirectly be measured. Due to the broader absorption lineshape, it is possible to saturate the restricted protons by an off-resonance RF pulse (43).

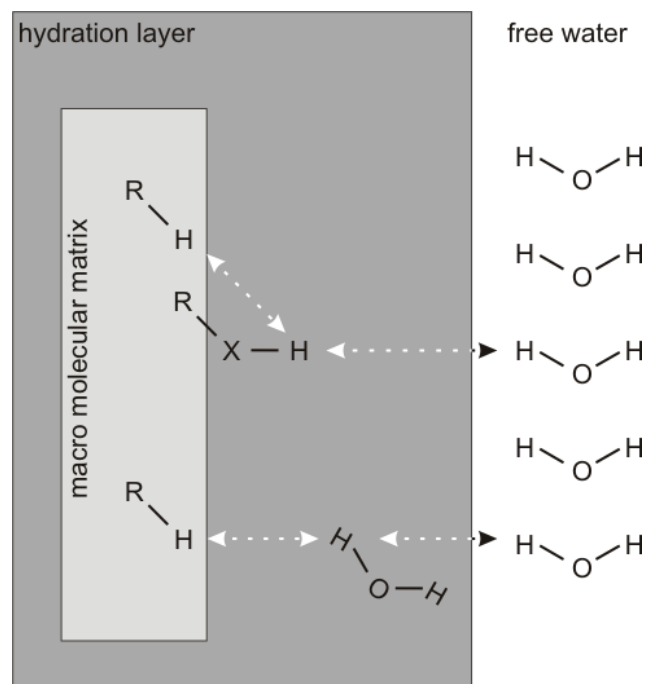


Figure 5. Schematic representation of the magnetization transfer effect. Magnetization can be transferred from the macro molecular matrix to the free water via two pathways, with or without the use of the water molecules in the hydration layer surrounding the macro molecular matrix.

The saturation is then transferred to the free water protons by MT, which leads to a signal reduction of the free water.

Especially in the bSSFP sequence, MT can severely reduce the obtained steady state signal intensity up to a factor of two (44). Within the bSSFP sequence, MT is more pronounced when using short TR and large flip angles, saturating the magnetization of the restricted pool protons (45,46).

Since the DESPOT2 method uses bSSFP acquisitions to determine the T_2 decay rate, the MT might bias the obtained T_2 value. It would thus be useful to reduce the MT effect to a minimum within the bSSFP sequence for T_2 determination. The signal reduction due to MT can be reduced by the use of elongated repetition time and reduced flip angles as indicated above. However, increased TR is not desired because of an increased acquisition time and invalidity of the linearization for $TR > 10$ ms nor is a change of flip angles acceptable because of a possible loss in T_2 precision (15). Only recently, a new way of MT effect reduction within a bSSFP sequence has been discovered. The use of long RF excitation pulses can also reduce the MT effect and almost completely remove the signal reduction in the bSSFP sequence due to MT without significant elongation of the scan time and without a change in flip angle.

Finite Pulse Effect

In the late 50s Carr (23) introduced that a steady state is established by a fast train of RF excitation pulses interleaved by periods of steady state free precession (SSFP). From their long history, signal equations for SSFP sequences are generally well accepted and unquestioned. SSFP signal equations derive from a piecewise constant, integrated Bloch equation, by a simple time evolution analysis. Instantaneous RF pulses are assumed within this analysis, neglecting relaxation effects during the RF pulse. Since for bSSFP sequences, minimal TR settings (typically in the range of 3 - 5 ms) are preferred to reduce banding artifacts (i.e., off-resonance voids appearing at π -multiples in phase cycled bSSFP), even short RF excitation pulses ($T_{RF} \sim 0.5 - 1$ ms) can take a severe fraction of the TR period. Clearly, in the limit of $T_{RF} \rightarrow 0$, the assumption of instantaneous RF pulses holds and the signal becomes independent of the RF pulse duration. However, when imaging brain tissue, one might want to avoid the MT effect by pulse elongation.

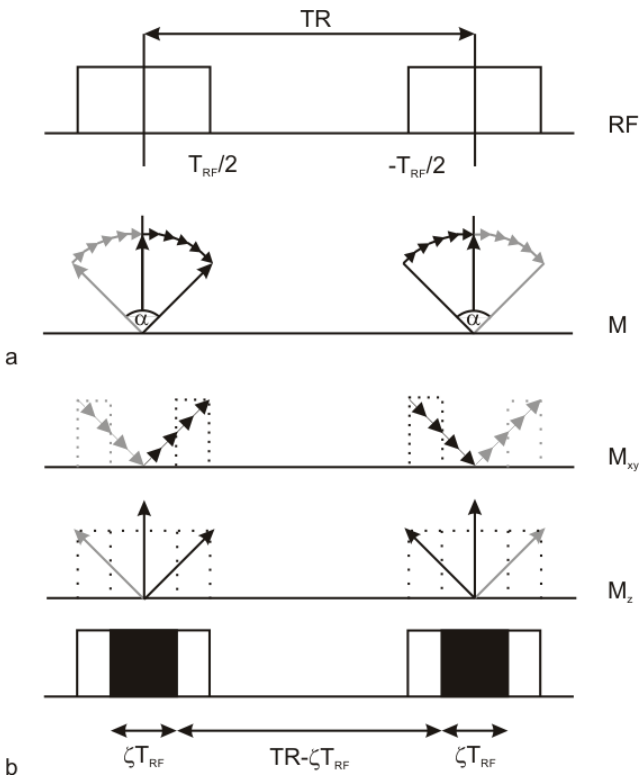


Figure 6. Schematic illustration of the steady state movement of the magnetization within an alternating phase bSSFP sequence using non selective RF pulses. On-resonant magnetization passes through the zenithal alignment when going from its initial to its final state (a). The transverse magnetization first decreases and then increases again continuously during the RF excitation pulse, thereby decreasing and increasing the T_2 effects (b, top). The excitation can be divided into periods of partial transversal and zenithal (longitudinal) orientation of the magnetization (b, middle and bottom). The mean effective fraction during which the magnetization is in the longitudinal direction is indicated by ζ . Adapted version from Fig. 1 in reference (48).

Hereby, the RF excitation pulse will constitute a significant fraction of TR and the finite pulse effect (i.e., relaxation during excitation) has to be taken into account.

The well known and commonly accepted bSSFP signal equation is previously given but will be restated here and gives the signal directly after the (alternating phase) RF excitation. For $TR \ll T_1$ and T_2 , partial integration of the piecewise constant Bloch equation assuming instantaneous acting RF pulses and solving for the steady state coherent solution leads to the equation presented by Perkins and Wehrli in 1986 (30):

$$M_{xy}^+ = M_0 \sin \alpha \frac{1 - e^{-TR/T_1}}{1 - e^{-TR/T_1} e^{-TR/T_2} - \dots} (e^{-TR/T_1} - e^{-TR/T_2}) \cos \alpha \quad [15]$$

The signal at a centered echo (i.e., $TE = TR/2$) (47) is defined as:

$$M_{xy}(t = TR/2) = M_{xy}^+ \sqrt{e^{-TR/T_2}} \quad [16]$$

In the case of elongated excitation pulses, e.g. to reduce MT, the above equations are not correctly describing the bSSFP signal due to the invalidity of the assumption of instantaneously acting RF pulses.

Finite RF pulse effect: Hard pulse excitation

For on-resonance alternating RF excitation pulses (i.e., $\pm\alpha$), the steady state magnetization describes a 'zenithal' movement: the magnetization passes along a fully longitudinal alignment when going from its initial onto its final position (Fig. 6). This leads to an overestimation of the duration of the transverse relaxation process within TR , since there is no T_2 decay during the zenithal period (i.e., the period the magnetization needs to pass along the longitudinal alignment; Fig. 6).

The finite RF excitation pulse can be considered to be composed of a series of equidistant small δ -pulses of zero duration. To leading order, the reduction of magnetization during each time interval between two δ -pulses (i.e., time interval: $[t_i, t_i + \delta t]$) is given by:

$$\delta M_{xy}(t_i) \approx -\frac{\delta t}{T_2} M_{xy}(t_i) \quad [17]$$

$$\delta M_x(t_i) \approx -\frac{\delta t}{T_1} (M_x(t_i) - M_0) \quad [18]$$

Here, the transverse steady state magnetization is indicated by M_{xy} and the longitudinal steady state magnetization by M_z . For sufficiently small flip angles ($\alpha \ll 180^\circ$), the relative weighting of transverse and longitudinal magnetization does not change significantly. Accumulation of relaxation during an RF pulse therefore only depends on the magnetization trajectory. The accumulated transverse magnetization decrease and longitudinal magnetization increase immediately after excitation is obtained after summation, which gives:

$$\Delta M_{xy}^+ \approx -\frac{T_{RF}}{T_2} \langle M_{xy} \rangle^+ \quad [19]$$

$$\Delta M_z^+ \approx -\frac{T_{RF}}{T_1} \left(\langle M_z \rangle^+ - M_0 \right) \quad [20]$$

where the time average of the trajectory is defined by:

$$\langle M_{xy,z} \rangle^+ := \frac{1}{T_{RF}} \int_0^{T_{RF}} M_{xy,z}(t) dt \quad [21]$$

Although the magnetization trajectory is additionally modified by T_1 and T_2 relaxation, this correction is in the order of $T_{RF}/T_{1,2}$, and in combination with Eq. 20 and 21 ignored. For sufficiently small flip angles ($\alpha \ll 180^\circ$), the time dependence of the trajectory is linear; for rectangular pulses, also the trajectory itself is linear, and therefore:

$$\langle M_{xy} \rangle^+ = 0.5 M_{xy}^- \quad [22]$$

and

$$\langle M_z \rangle^+ = \frac{\sin(\alpha/2)}{\alpha/2} M_z^- \approx M_z^- \quad [23]$$

where the $-$ indicates the magnetization immediately before the RF pulse. Only within the transverse magnetization, a considerable change in magnetization is observed, while the longitudinal magnetization is only marginally affected. The difference between the pre- and post-pulse transverse magnetization is captured in ζ as follows from Eq. 24 and the definition

$$\langle M_{xy} \rangle^+ = (1-\zeta) M_{xy}^- \quad [24]$$

Therefore, the accumulated finite pulse effects are of form:

$$\Delta M_{xy}^+ \approx -\frac{(1-\zeta)T_{RF}}{T_2} M_{xy}^- \quad [25]$$

$$\Delta M_z^+ \approx -\frac{T_{RF}}{T_1} (M_z^- - M_0) \quad [26]$$

These results can be interpreted as:

1. Only the transverse magnetization is affected by finite RF pulses;
2. During ζT_{RF} , no transverse relaxation occurs. Therefore, the effective duration of the RF pulse is reduced by a factor $(1-\zeta)$;
3. The period ζT_{RF} can pictorially be taken as the mean effective zenithal residence time during which the magnetization is in longitudinal orientation (Fig. 6).

To the order of $T_{RF}/T_{1,2}$ and for the special trajectory as generated by the bSSFP sequence with alternating phase, the differential form of relaxation within a finite RF excitation pulse reads:

$$\frac{dM_{xy}(t)}{dt} = -\frac{1-\zeta}{T_2} M_{xy}(t) \quad [27]$$

$$\frac{dM_z(t)}{dt} = \frac{1}{T_1} (M_z(t) - M_0) \quad [28]$$

From this, the common SSFP relaxation terms during TR are of the form:

$$\left. \begin{array}{l} E_1 := e^{-TR/T_1} \\ E_2 := e^{-TR/T_2} \end{array} \right\} \longrightarrow \left\{ \begin{array}{l} E_1 := e^{-TR/T_1} \\ E_2 := e^{-(TR-\zeta T_{RF})/T_2} \end{array} \right. \quad [29]$$

E_2 is thus increased by elongated finite pulse duration (i.e., effective reduction of TR). This was formerly captured as an effective increase in T_2 in order to maintain the general $E_{1,2}$ framework without the incorporated finite pulse correction (Eq. 29). For the general framework, to leading order, no correction for finite pulses is necessary for E_1 , since longitudinal components are not affected by finite pulse effects.

Finite RF pulse effect: Selective excitation

By defining a hard pulse equivalent for a slice selective excitation pulse, the above proposed substitution in E_2 is transferred from hard pulse to common slice selective excitation pulses (i.e., excitation

pulses with time varying amplitude $B_1(t)$ and duration T_{RF}). The hard pulse equivalent will have constant mean amplitude $\langle B \rangle$ and an effective RF pulse duration T_{RFE} , such that:

$$T_{RFE} \langle B \rangle = \int B_1(t) dt \quad [30]$$

This simply states the requirement of identical flip angles for the slice selective excitation and its hard pulse equivalent. The difficult or tricky part is the calculation of a time averaged magnetization trajectory for an arbitrary pulse shape. Bieri and Scheffler (48) have presented the calculation of a hard pulse equivalent for a frequently used slice selective excitation pulse of Gaussian shape. The duration of the hard pulse equivalent relates to the Gaussian time-bandwidth (TBW) product and pulse duration according:

$$T_{RFE} = \frac{8\sqrt{\log(2)}}{\pi\sqrt{\pi}} \frac{T_{RF}}{TBW} \approx \dots \quad [31]$$

$$1.20 \frac{T_{RF}}{TBW}$$

For short hand notation, the reduction in TR can be captured in the definition of R_2 (i.e., $1/T_2$), leading to:

$$\widetilde{E}_2 := e^{-TR \cdot R_2}, \widetilde{R}_2 := \dots \quad [32]$$

$$\left(1 - \zeta \frac{T_{RFE}}{TR}\right) R_2 \Rightarrow \widetilde{T}_2 > T_2$$

Thus, when expanding the definition of the hard pulse equivalent for Gaussian pulses to hard pulses leads to:

$$T_{RFE} \begin{cases} T_{RF} & : \text{hard pulses} \\ 1.20 \frac{T_{RF}}{TBW} & : \text{Gaussian pulses} \end{cases} \quad [33]$$

For other pulse shapes than hard pulses and Gaussian pulses, the effective pulse duration has to be recalculated to create the correct hard pulse equivalent for that specific pulse.

Multiple T_1 and T_2 combinations

The proposition of a single T_1 and T_2 combination in the SE and DESPOT2 T_2 quantifications overlook the complex microstructural organization of tissue. Analysis of transversal relaxation data has shown considerable promise for clarification of tissue microstructure by decomposition of the

measured signal into multiple components, each believed to come from distinct tissue subdomains (49-60). T_2 data obtained from a variety of neural tissue has proven the existence of at least two relaxation components: a fast relaxing component with $T_2 < 50$ ms, and a slower relaxing component with $T_2 > 70$ ms (15,56,57,61-63). Based on histological correlations (62,63), the fast relaxing component is broadly attributed to water trapped between myelin sheaths, while the slower relaxing component is believed to be from the free water in the intra- and extracellular pools. This is further supported by the correspondence between a decrease in the amplitude of the fast relaxing species' volume fraction and a decrease in myelination (64) as well as by its absence in nonmyelinated tissue samples (65). Similar observations of multicomponent T_2 relaxation have been observed in skeletal muscle (66,67) and articular cartilage (68), also resulting from differing physical environments in the tissue.

Myelin is an electrically insulating material that consists of multiple lipid bilayers surrounding the axons of neurons and mainly appears in white matter, and to a smaller amount in gray matter of the peripheral and central nervous system of vertebrates. The main function of the myelin sheaths is to improve the electrical signal conduction along the axon by increasing its velocity. Myelin sheaths tightly enclose water, which therefore experiences shorter relaxation times than inter- and intracellular water.

A two pool model can describe the gray and white matter tissue including the free water as well as the water trapped between the myelin sheaths. A fast relaxing pool represents the water trapped in between the myelin sheaths (abbreviation f , Fig. 7) while a slow pool represents the free water in the inter- and intracellular pools (abbreviation s ; Fig. 7). The proton exchange between the two pools is additionally included to the model. The relaxation parameters T_1 and T_2 of the two pools as well as the

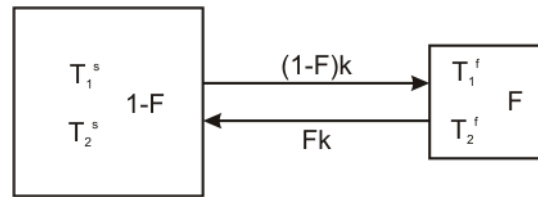


Figure 7. Coupled two-compartment model with the physical properties specifying the system. The properties of the slow pool are indicated by the indices s (left) and those of the fast pool with the indices f (right). The fast pool fraction equals F , and the slow pool fraction $1-F$. The direction dependent exchange rates are proportional to the pool fractions.

pool fractions F (fast pool fraction) and $1-F$ (slow pool fraction) and the exchange rate k characterize the tissue simulated by the model.

The magnetization of the fast pool (M_f) will decrease by $(1-F)k M_f$ and increase by $Fk M_s$. Similar to this, the magnetization of the slow pool (M_s) will drop by $Fk M_s$ and rise by $(1-F)k M_f$. Written in the differential form, this becomes:

$$\frac{dM^s}{dt} = -(1-F)kM^s + FkM^f \quad [34]$$

$$\frac{dM^f}{dt} = -FkM^f + (1-F)kM^s \quad [35]$$

Incorporating this exchange to the 6D Bloch equations (69) describing a decoupled two pool model, makes the modified 6D Bloch equations describe the magnetization change of a coupled two pool system.

Although multicomponent T_2 quantification studies have clinical application in demyelinating disorders such as multiple sclerosis (57,63), an obstacle of significance to widespread adoption is the lengthy acquisition times associated with these methods.

Other mechanisms

Next to the previously described mechanisms, more mechanisms influencing the outcome of T_2 quantification exist. Although they will not be described in detail here, their influence might be significant. Change in magnetic properties due to oxygenation or de-oxygenation of hemoglobin (the BOLD effect; (70)). Diffusion (71) and perfusion can also affect the observed relaxation times. Although these are important mechanisms, they go beyond the investigated and are therefore not further explained.

AIM OF THIS THESIS

The absolute determination of T_2 has shown to be clinically useful in areas such as the diagnosis of epilepsy (3), determination of the severity of Parkinson's disease (4). Also schizophrenia (2), multiple sclerosis (6), and other diseases have demonstrated variations in T_2 within specific brain regions. Despite the clinical relevance of volumetric T_2 quantification, it is not part of the routine clinical assessment, likely due to the long scan times and low resolution associated with conventional mapping methods.

A method rapidly determining T_2 in an accurate and precise manner would therefore be very welcome. Deoni et al. presented a method, the DESPOT2 method (15), based on the variable nutation angle method originally introduced in the 70s by Christensen et al. (34). Deoni et al. have proven in 2005 (72) that this method is capable of acquiring both a whole-brain T_1 and T_2 map of 1 mm isotropic resolution within less than 17 minutes. This is clinically seen a very well acceptable acquisition time. Therefore, this new method might lead to volumetric T_2 quantification to be part of the routine clinical assessment.

Despite the long acquisition time, spin echo (SE) and multi echo spin echo (mSE) remain the principle T_2 mapping methods up to now. Before the DESPOT2 method might become accepted within the clinical routine assessment, it has to be proven that it is equally stable as the principle methods used so far. When finally accepted, it might take the place of the spin echo method now seen as the standard in T_2 quantification.

When measuring tissue with the bSSFP sequence as the DESPOT2 method requires, inherent magnetization transfer (MT) contrast is acquired. It is known that the obtained signal is therefore not conform to the theoretical description as used within the DESPOT2 method. This issue has to be investigated and solved before clinical acceptance of the method.

In this thesis, this is done by the use of elongated RF pulse durations minimizing the MT effect. The elongated RF pulse duration on its turn introduces finite pulse effects leading to an overestimation of T_2 . This can be corrected for within the T_2 calculation of the DESPOT2 method, as presented in this thesis.

Next to the exchange of magnetization by the MT effect, there is also the presence of complex microstructural organization of tissue consisting of

(coupled) multiple T_1 and T_2 combinations. A good example is the exchange of magnetization between the water trapped in the myelin sheaths and the free water in inter- and intracellular pools. The proposition of single T_1 and T_2 combination of both the SE and the DESPOT2 overlook this. It is investigated how the fractions of two compartments with different T_1 and T_2 as well as their exchange rate influence the outcome of both methods.

The goal of this thesis is to test the capabilities of the DESPOT2 of becoming the new principle technique for (volumetric) T_2 quantification of brain tissue. For this reason, simulations as well as measurements on phantoms and healthy volunteers are considered in this work.

OUTLINE OF THE THESIS

Within **chapter 2**, the influence of RF pulse elongation for reduction of MT is investigated by means of numerical simulations and measurements. The analytical solution to a binary spin-bath model is used for the simulation of the MT effect in tissue as previously derived by Gloor et al. (46). Within the simulations the RF pulse duration is varied, due to which TR is elongated (i.e., due to minimal TR settings, elongation of any part of the sequence will elongate TR). To exclude signal dependency on TR , a delay was implemented to result in identical TR settings for each used T_{RF} . Within the experiments, the implemented delay was also used, ensuring constant TR in all bSSFP acquisitions. Results from both the simulations and the measurements show that there is a significant influence of MT on the obtained T_2 by the DESPOT2 method. For short RF pulse durations, a reduced T_2 is observed due to the MT effect. Since the investigation of the MT effect on the DESPOT2 method showed to be severe, the use of elongated pulse duration is advised to reduce MT.

The elongated pulse duration advised in chapter 2 introduces finite pulse effects. These effects are not accounted for in the DESPOT2 T_2 quantification as presented by Deoni et al. (15,72). **Chapter 3** describes the implementation of finite pulse effect correction in the DESPOT2 T_2 quantification equation. By means of a single-pool and a two-pool model, the severity of the finite pulse effect is indicated and the influence of the correction for finite pulse effects clearly shown. Although one can correct for finite pulse effects, the MT influence as shown in chapter 1 is still present in case of short RF pulse durations. Measurement results describe identical successful results for the correction of finite pulse effects: the obtained T_2 no longer depends on the RF pulse duration. In phantom measurements, perfect correspondence between the mSE results and the corrected DESPOT2 results for all RF pulse durations was obtained. However, although the dependence on the RF pulse duration has been departed and long RF pulses were used to avoid MT effect, an underestimation compared to the SE based T_2 observation has been seen; however, the obtained DESPOT2 result corresponds to values of a two-pool analysis presented in other literature. It is shown that by a simple modification of the linearized signal equation used in the DESPOT2 method, the method becomes insensitive to variations in RF pulse duration. To over-

come MT influences on the obtained T_2 , RF pulse elongation can now be applied without any further consequences.

The structural underestimation obtained in the brain measurements with DESPOT2 compared to the SE measurements based T_2 observation is further investigated in **chapter 4**. The overlooked microscopic complexity of brain tissue, a coupled two pool system, might actually influence both the SE and DESPOT2 observed T_2 and therefore be the cause of the obtained underestimation. A coupled two pool water model and the modified 6 dimensional modified Bloch equations (56) are used to simulate the signal for SE, SPGR and bSSFP sequences. Gray and white matter parameters as published in (73) have been used to simulate these brain tissues and investigate the influence of the coupled two pool system. These parameters describe the myelin water versus free water system; besides the different relaxation times of the two tissues, pool fractions and exchange rates also differ.

The general thought that the equal echo spacing within the (m)SE sequence for T_2 quantification influences the observed single T_2 of a two- T_2 probe has shown to be false in the case of a coupled two pool system measured with equidistant echoes. Here, the echo spacing is of negligible influence on the outcome. The time span over which the data points are distributed (i.e., shortest TE – longest TE) has to be equally long as, or longer than the T_2 observed. Otherwise large reduction of the observed T_2 results due to extremely heavy weighting of the fast pool. However, this restriction on the time span is generally well accepted and applied with the SE T_2 quantification approach.

For both gray and white matter, the flip angle choices of the bSSFP sequence have been investigated. The results have shown that severe dependence of the obtained T_2 on the flip angle choice exists. For the flip angles supposed to have optimal T_2 precision (15) significant underestimations are observed. Since several diseases affect the pool size fraction as well as the exchange rates, their influence on the observed T_2 difference between SE and DESPOT2 approaches was investigated by simulations. The influence on the pool size fractions has shown to be of greater influence than the exchange rate. It is again shown that for the single compartment situation both methods result in identical T_2 observation. However, with the suggested flip angle choice for optimal T_2 precision, T_2 is underestimated by DESPOT2 compared to the SE observed T_2 for all pool size fractions and exchange rates.

Hereby, the underestimation observed in chapter 3 can be explained by single T_2 observation of a coupled two pool system.

REFERENCES

1. Friedman SD, Shaw DW, Artru AA, Richards TL, Gardner J, Dawson G, Posse S, Dager SR. Regional brain chemical alterations in young children with autism spectrum disorder. *Neurology* 2003;60(1):100-107.
2. Williamson P, Pelz D, Merskey H, Morrison S, Karlik S, Drost D, Carr T, Conlon P. Frontal, temporal, and striatal proton relaxation times in schizophrenic patients and normal comparison subjects. *Am J Psychiatry* 1992;149(4):549-551.
3. Pitkanen A, Laakso M, Kalviainen R, Partanen K, Vainio P, Lehtovirta M, Riekkinen P, Soininen H. Severity of hippocampal atrophy correlates with the prolongation of MRI T2 relaxation time in temporal lobe epilepsy but not in Alzheimer's disease. *Neurology* 1996;46(6):1724-1730.
4. Bartzokis G, Sultzer D, Cummings J, Holt LE, Hance DB, Henderson VW, Mintz J. In vivo evaluation of brain iron in Alzheimer disease using magnetic resonance imaging. *Arch Gen Psychiatry* 2000;57(1):47-53.
5. Vymazal J, Righini A, Brooks RA, Canesi M, Mariani C, Leonardi M, Pezzoli G. T1 and T2 in the brain of healthy subjects, patients with Parkinson disease, and patients with multiple system atrophy: relation to iron content. *Radiology* 1999;211(2):489-495.
6. Larsson HB, Frederiksen J, Petersen J, Nordenbo A, Zeeberg I, Henriksen O, Olesen J. Assessment of demyelination, edema, and gliosis by in vivo determination of T1 and T2 in the brain of patients with acute attack of multiple sclerosis. *Magn Reson Med* 1989;11(3):337-348.
7. Detre JA, Leigh JS, Williams DS, Koretsky AP. Perfusion imaging. *Magn Reson Med* 1992;23(1):37-45.
8. Gowland P, Mansfield P, Bullock P, Stehling M, Worthington B, Firth J. Dynamic studies of gadolinium uptake in brain tumors using inversion-recovery echo-planar imaging. *Magn Reson Med* 1992;26(2):241-258.
9. Carr HY, Purcell EM. Effects of diffusion on free precession in nuclear magnetic resonance experiments. *Physiological Reviews* 1954;94:630.
10. Meiboom S, Purcell EM. Modified spin-echo method for measuring nuclear relaxation times. *The Review of scientific instruments* 1958;29:688-691.
11. Deichmann R, Adolf H, Noth U, Morrissey S, Schwarzbauer C, Haase A. Fast T2-mapping with snapshot flash imaging. *Magn Reson Imaging* 1995;13(4):633-639.
12. Gneiting T, Nekolla S, Syha J, Keinlin MV, Haase A. Fast T2 imaging with Carr-Purcell Snapshot-FLASH. 1992; New York. p 1346.
13. Schmitt P, Griswold MA, Jakob PM, Kotas M, Gulani V, Flentje M, Haase A. Inversion recovery TrueFISP: quantification of T(1), T(2), and spin density. *Magn Reson Med* 2004;51(4):661-667.
14. Bieri O, Scheffler K, Welsch GH, Trattnig S, Mamisch TC, Ganter C. Quantitative mapping of T(2) using partial spoiling. *Magn Reson Med* 2011; 000:000-000.
15. Deoni SC, Rutt BK, Peters TM. Rapid combined T1 and T2 mapping using gradient recalled acquisition in the steady state. *Magn Reson Med* 2003;49(3):515-526.
16. Bernstein MA, King KF, Zhou JZ. Handbook of MRI Pulse Sequences: Elsevier Academic Press; 2004.
17. Haacke EM, Brown RW, Thompson MR, Venkatesan R. Magnetic Resonance Imaging: Physical Principles and Sequence Design: John Wiley & Sons, Inc.; 1999.
18. Gyngell ML, Palmer ND, Eastwood LM. The application of steady-state free precession in 2D-FT MR Imaging. 1986; Montreal, Canada.
19. Zur Y, Wood ML, Neuringer LJ. Spoiling of transverse magnetization in steady-state sequences. *Magn Reson Med* 1991;21(2):251-263.
20. Sobol WT, Gauntt DM. On the stationary states in gradient echo imaging. *J Magn Reson Imaging* 1996;6(2):384-398.
21. Scheffler K. A pictorial description of steady-states in rapid magnetic resonance imaging. *Concepts in Magnetic Resonance* 1999;11(5):291-304.
22. Ernst RR, Bodenhausen G, Wokaun A. Principles of nuclear magnetic resonance in one and two dimensions. Oxford: Clarendon Press; 1987.

23. Carr HY. Steady-state free precession in nuclear magnetic resonance. *Phys Rev* 1958;112(5):1693-1701.
24. Freeman R, Hill HDW. Phase and intensity anomalies in fourier transform. *J Magn Reson* 1971;4:366-383.
25. Hinshaw WS. Image formation by nuclear magnetic resonance: the sensitive-point method. *J Appl Phys* 1976;47:3709-3721.
26. Zur Y, Stokar S, Bendel P. An analysis of fast imaging sequences with steady-state transverse magnetization refocusing. *Magn Reson Med* 1988;6(2):175-193.
27. Hendrick RE, Kneeland JB, Stark DD. Maximizing signal-to-noise and contrast-to-noise ratios in FLASH imaging. *Magn Reson Imag* 1987;5:117-127.
28. Young IR, Burl M, Bydder GM. Comparative efficiency of different pulse sequences in MR imaging. *J Comput Assist Tomogr* 1986;10:271-285.
29. Hawkes RC, Patx S. Rapid Fourier imaging using steady-state free precession. *Magn Reson Med* 1987;4:9-23.
30. Perkins TG, Wehrli FW. CSF signal enhancement in short TR gradient echo images. *Magn Reson Imag* 1986;4:465-467.
31. Buxton RB, Fisel CR, Chien D, Brady TJ. Signal intensity in fast NMR imaging with short repetition times. *J Magn Reson* 1989;83:576-585.
32. Lebel RM, Wilman AH. Transverse relaxometry with stimulated echo compensation. *Magn Reson Med*;64(4):1005-1014.
33. Bluml S, Schad LR, Stepanow B, Lorenz WJ. Spin-lattice relaxation time measurement by means of a TurboFLASH technique. *Magn Reson Med* 1993;30(3):289-295.
34. Christensen KA, Grand DM, Schulman EM, Walling C. Optimal determination of relaxation times of Fourier transform nuclear magnetic resonance. Determination of spin-lattice relaxation times in chemically polarized species. *J Phys Chem* 1974;78:1971-1977.
35. Wang HZ, Riederer SJ, Lee JN. Optimizing the precision in T1 relaxation estimation using limited flip angles. *Magn Reson Med* 1987;5:399-416.
36. Homer J, Beevers MS. Driven-equilibrium single-pulse observation of T1 relaxation. A re-evaluation of a rapid 'new' method for determining NMR spin-lattice relaxation times. *J Magn Reson* 1985;63:287-297.
37. Homer J, Roberts JK. Conditions for the driven equilibrium single pulse observation of spin-lattice relaxation times. *J Magn Reson* 1987;74:424-432.
38. Homer J, Roberts JK. Routine evaluation of M0 ratios and T1 values from driven equilibrium NMR spectra. *J Magn Reson* 1990;87:265-272.
39. Eng J, Ceckler TL, Balaban RS. Quantitative 1H magnetization transfer imaging in vivo. *Magn Reson Med* 1991;17(2):304-314.
40. Ceckler T, Maneval J, Melkowitz B. Modeling magnetization transfer using a three-pool model and physically meaningful constraints on the fitting parameters. *J Magn Reson* 2001;151(1):9-27.
41. Liepinsh E, Otting G. Proton exchange rates from amino acid side chains--implications for image contrast. *Magn Reson Med* 1996;35(1):30-42.
42. Fralix TA, Ceckler TL, Wolff SD, Simon SA, Balaban RS. Lipid bilayer and water proton magnetization transfer: effect of cholesterol. *Magn Reson Med* 1991;18(1):214-223.
43. Doussset V, Grossman RI, Ramer KN, Schnall MD, Young LH, Gonzalez-Scarano F, Lavi E, Cohen JA. Experimental allergic encephalomyelitis and multiple sclerosis: lesion characterization with magnetization transfer imaging. *Radiology* 1992;182(2):483-491.
44. Bieri O, Scheffler K. On the origin of apparent low tissue signals in balanced SSFP. *Magn Reson Med* 2006;56(5):1067-1074.
45. Bieri O, Scheffler K. Optimized balanced steady-state free precession magnetization transfer imaging. *Magn Reson Med* 2007;58(3):511-518.
46. Gloor M, Scheffler K, Bieri O. Quantitative magnetization transfer imaging using balanced SSFP. *Magn Reson Med* 2008;60(3):691-700.
47. Scheffler K, Hennig J. Is TrueFISP a gradient-echo or a spin-echo sequence? *Magn Reson Med* 2003;49(2):395-397.

48. Bieri O, Scheffler K. SSFP signal with finite RF pulses. *Magn Reson Med* 2009;62(5):1232-1241.
49. Kroeker RM, Henkelman RM. Analysis of Biological NMR Relaxation Data with Continuous Distributions of Relaxation Times. *J Magn Reson* 1986;69:218-235.
50. Armspach JP, Gounot D, Rumbach L, Chambron J. In vivo determination of multiexponential T2 relaxation in the brain of patients with multiple sclerosis. *Magn Reson Imaging* 1991;9(1):107-113.
51. Menon RS, Rusinko MS, Allen PS. Multiexponential proton relaxation in model cellular systems. *Magn Reson Med* 1991;20(2):196-213.
52. Cheng KH. In vivo tissue characterization of human brain by chi-squares parameter maps: multiparameter proton T2-relaxation analysis. *Magn Reson Imaging* 1994;12(7):1099-1109.
53. Whittall KP, MacKay AL, Graeb DA, Nugent RA, Li DK, Paty DW. In vivo measurement of T2 distributions and water contents in normal human brain. *Magn Reson Med* 1997;37(1):34-43.
54. Stanisiz GJ, Kecojevic A, Bronskill MJ, Henkelman RM. Characterizing white matter with magnetization transfer and T(2). *Magn Reson Med* 1999;42(6):1128-1136.
55. Kreis R, Fusch C, Boesch C. In vivo measurement of T2 distributions and water contents in normal human brain. 1992; Berlin, Germany.
56. Lenz C, Klarhofer M, Scheffler K. Limitations of rapid myelin water quantification using 3D bSSFP. *MAGMA*;23(3):139-151.
57. MacKay A, Laule C, Vavasour I, Bjarnason T, Kolind S, Madler B. Insights into brain microstructure from the T2 distribution. *Magn Reson Imaging* 2006;24(4):515-525.
58. Menon RS, Allen PS. Application of continuous relaxation time distributions to the fitting of data from model systems and excised tissue. *Magn Reson Med* 1991;20(2):214-227.
59. Stewart WA, MacKay AL, Whittall KP, Moore GR, Paty DW. Spin-spin relaxation in experimental allergic encephalomyelitis. Analysis of CPMG data using a non-linear least squares method and linear inverse theory. *Magn Reson Med* 1993;29(6):767-775.
60. Vasilescu V, Katona E, Simplaceanu V, Demco D. Water compartments in the myelinated nerve. III. *Pulsed NMR results. Experientia* 1978;34(11):1443-1444.
61. Deoni SC, Rutt BK, Jones DK. Investigating exchange and multicomponent relaxation in fully-balanced steady-state free precession imaging. *J Magn Reson Imaging* 2008;27(6):1421-1429.
62. Gareau PJ, Rutt BK, Karlik SJ, Mitchell JR. Magnetization transfer and multi-component T2 relaxation measurements with histopathologic correlation in an experimental model of MS. *J Magn Reson Imaging* 2000;11(6):586-595.
63. Laule C, Leung E, Li DK, Traboulsee AL, Paty DW, MacKay AL, Moore GR. Myelin water imaging in multiple sclerosis: quantitative correlations with histopathology. *Mult Scler* 2006;12(6):747-753.
64. MacKay A, Whittall K, Adler J, Li D, Paty D, Graeb D. In vivo visualization of myelin water in brain by magnetic resonance. *Magn Reson Med* 1994;31(6):673-677.
65. Beaulieu C, Fenrich FR, Allen PS. Multi-component water proton transverse relaxation and T2-discriminated water diffusion in myelinated and nonmyelinated nerve. *Magn Reson Imaging* 1998;16(10):1201-1210.
66. Hazlewood CF, Chang DC, Nichols BL, Woessner DE. Nuclear magnetic resonance transverse relaxation times of water protons in skeletal muscle. *Biophys J* 1974;14(8):583-606.
67. Saab G, Thompson RT, Marsh GD. Multi-component T2 relaxation of in vivo skeletal muscle. *Magn Reson Med* 1999;42(1):150-157.
68. Mosher TJ, Chen Q, Smith MB. 1H magnetic resonance spectroscopy of nanomelic chicken cartilage: effect of aggrecan depletion on cartilage T2. *Osteoarthritis Cartilage* 2003;11(10):709-715.
69. Bloch F. Nuclear Induction. *Phys Rev* 1946;70:460-474.
70. Thulborn KR, Waterton JC, Matthews PM, Radda GK. Oxygenation dependence of the transverse relaxation time of water protons in whole blood at high field. *Biochim Biophys Acta* 1982;714(2):265-270.

71. Stejskal EO, Tanner JE. Spin diffusion measurements: Spin echoes in the presence of a time-dependent field gradient. *J Chem Phys* 1965;42:288.
72. Deoni SC, Peters TM, Rutt BK. High-resolution T1 and T2 mapping of the brain in a clinically acceptable time with DESPOT1 and DESPOT2. *Magn Reson Med* 2005;53(1):237-241.
73. Deoni SC, Rutt BK, Arun T, Pierpaoli C, Jones DK. Gleaning multicomponent T1 and T2 information from steady-state imaging data. *Magn Reson Med* 2008;60(6):1372-1387.

2

Influence Of MT Effects On T_2 Quantification With 3D Balanced Steady-State Free Precession Imaging

Signal from balanced steady-state free precession is affected by magnetization transfer. To investigate the possible effects on derived T_2 values using variable nutation steady-state free precession, magnetization transfer-effects were modulated by varying the radiofrequency pulse duration only or in combination with variable pulse repetition time. Simulations reveal a clear magnetization transfer dependency of T_2 when decreasing radiofrequency pulse duration, reaching maximal deviation of 34.6% underestimation with rectangular pulses of 300 ms duration. The observed T_2 deviation evaluated in the frontal white matter and caudate nucleus shows a larger underestimation than expected by numerical simulations. However, this observed difference between simulation and measurement is also observed in an aqueous probe and can therefore not be attributed to magnetization transfer: it is an unexpected sensitivity of derived T_2 to radiofrequency pulse modulation. As expected, the limit of sufficiently long radiofrequency pulse duration to suppress magnetization transfer-related signal modulations allows for proper T_2 estimation with variable nutation steady-state free precession.

An adapted version of this chapter has been published as: H.J.A. Crooijmans, M. Gloor, O. Bieri, and K. Scheffler. Influence Of MT On T_2 Quantification With 3D Balanced Steady-State Free Precession Imaging. *Magn Reson Med*, 65(1):195-201, 2010

INTRODUCTION

A variety of different quantitative T_2 MRI techniques has been developed over the years (single-echo spin-echo, multiecho spin-echo, and T_2 preparation with spiral or SPGR readout). In contrast to common single spin-echo or multicontrast spin-echo sequences, quantification of T_2 using steady-state free precession (SSFP) sequences, such as inversion recovery SSFP (1) or variable nutation SSFP (radiofrequency (RF) spoiled SSFP-free induction decay (FID): driven equilibrium single-pulse observation of T_1 (DESPOT1); and balanced SSFP: driven equilibrium single-pulse observation of T_2 (DESPOT2) (2) is considerably faster.

DESPOT2 is based on the acquisition of (i) two RF spoiled gradient echoes and (ii) two fully balanced SSFP (bSSFP) images (3). To calculate T_2 , T_1 is first extracted from the two spoiled gradient echo images acquired with constant pulse repetition time (TR) and varied flip angle (α) through a linearization of the signal, as described in Christensen et al. (4). This T_1 information, combined with the data from multiple bSSFP images, also acquired with constant TR and varied α , allows a calculation of T_2 through a similar linearization of the bSSFP signal (2). Maximized estimate precision is achieved by a flip angle choice, as described in Deoni et al. (5), and can be established for both T_1 and T_2 (5).

It is generally well accepted that signal formation in bSSFP can be derived from the Freeman-Hill formulae (6), being proportional to $\sqrt{T_2/T_1}$ for repetition times $TR \ll T_1$; T_2 (7). However, it was only recently that signal deviations from the Freeman-Hill formulae indicated further contrast mechanisms, specifically that the steady-state of bSSFP in tissues may be reduced by up to a factor of 2 through magnetization transfer (MT) effects (8). MT is the exchange of spin magnetization between free water protons (free pool protons) and macromolecular protons in biologic systems (restricted pool protons) (9). In bSSFP, MT is more pronounced when using short TR s in combination with large flip angles, saturating the magnetization of restricted pool protons (10). Subsequent exchange of these protons with free pool protons constituting the steady state leads to an overall signal reduction compared to a situation without exchange due to MT effects. As a result, increasing deviations from the Freeman-Hill formulae might be expected with increasing flip angles, putting into question the accuracy of variable-flip-angle SSFP for tissues that

exhibit considerable MT effect, such as gray and white matter.

It has already been demonstrated by Ou and Gochberg (11) that MT can affect the DESPOT1 outcome. In another previous study by Zu et al. (10), it has also been demonstrated that MT effects may indeed also affect the DESPOT2 outcome in white matter. They advise the use of flip angles (α) of 25° and 80° to avoid this effect. This guidance is based on equal ratios of the signal intensity with MT effect to signal intensity without MT effect. However, this can only be achieved for one single tissue per acquisition. In contrast to Zu et al. (10), the present work will show and describe the signal intensity and the derived T_2 in several tissues for a range of RF pulse durations (T_{RF}), while the TR is kept constant by an implemented variable delay time, rather than using a variation of flip angles or TR . This is done to show the effect of a change in T_{RF} solely on the outcome. Both simulation and experimental data prove that MT affects the derived T_2 by DESPOT2 unless RF pulses of sufficient length are used; long pulses are pulses with $T_{RF} > \sim 1000$ ms for rectangular pulses and $T_{RF} > \sim 2500$ ms for sinc pulses with a time-bandwidth product of 2.7 (12). Within the limit of sufficiently long RF pulses, the simple one-pool model for bSSFP is restored to follow the Freeman-Hill formulae, and therefore, in this limit, the DESPOT2 method is suited to yield a proper estimate for T_2 .

MATERIALS AND METHODS

Experiments were performed on a Siemens 1.5T Avanto system (Siemens Healthcare, Erlangen, Germany), and numerical simulations, data analysis, and visualization were done in Matlab R2007b (The MathWorks, Inc., Natick, MA). MT ratio (MTR) plots were generated and statistical analysis was performed in Microsoft Excel 2007 (Microsoft Corporation, Redmond, WA).

Numerical Simulations

The MT effect in tissue can be modeled with a binary spin-bath model (13,14). Typically, saturation of restricted pool protons is achieved by off-resonance irradiation (frequency offset Δ) that ideally leaves the magnetization of free pool protons unaffected. Based on the assumption that fractional pool size modifications are negligible within TR (15), an analytical solution to the two-pool bSSFP model has been derived (15). Besides common sequence characteristics (α , T_{RF} , TR) and relaxation processes (T_1 and T_2), this equation is a function of the bound proton fraction F and exchange rate k_f . For excitation, both sinc and rectangular RF pulses of variable duration were used, and relaxation within the pulse duration was taken into account. The mean saturation rate ($\langle W \rangle$) is calculated as a function of α and T_{RF} based on a super-Lorentzian line shape $G(\Delta)$ being appropriate for the description of tissues (14,16). The on-resonance singularity is handled by extrapolating $G(\Delta)$ from about 1 kHz to the asymptotic limit $\Delta \rightarrow 0$, yielding $G(0) = 1.4 \cdot 10^{-5} \text{ sec}^{-1}$ (8,15) for $T_{2,r} = 12 \mu\text{s}$ (14). Due to the general uncertainty, no distinction is made between $G(0)$ for white matter and $G(0)$ for gray matter. The relaxation rate of the restricted pool $R_{1,r}$ is set equal to the one of the free pool $R_{1,f}$. Relaxation times and two-pool model parameters were assumed to be $T_{1,f} = 733 \text{ ms}$, $T_{2,f} = 40 \text{ ms}$, $F = 14.5\%$, $k_f = 4.5 \text{ sec}^{-1}$ for the frontal lobes, and $T_{1,f} = 1087 \text{ ms}$, $T_{2,f} = 59 \text{ ms}$, $F = 6.5\%$, $k_f = 2.3 \text{ sec}^{-1}$ for the caudate nucleus (15). Simulations are performed for the standard bSSFP sequence scheme (variable TR) and the sequence scheme where a built-in delay preserves a constant TR (Fig. 1).

Experiments

Two sets of experiments were performed: the first set on an MT-free phantom (sphere with a diameter of 64 mm, filled with 1 mM gadolinium in water) and the second set on a healthy volunteer, showing the influence of MT (typically, frequency shifts of

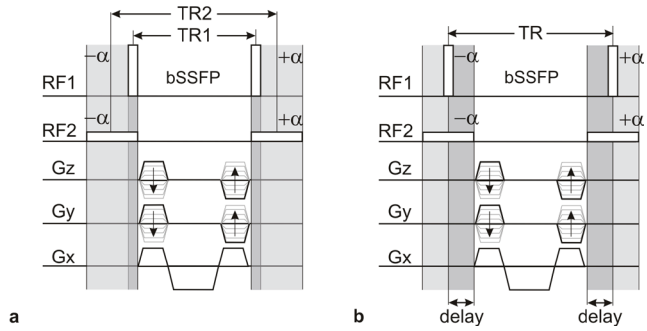


Figure 1. Three-dimensional bSSFP sequence schemes with rectangular excitation pulses using variable TR (a) and constant TR (b). The sequence with variable TR (a) was used for the simulation only, while the sequence with constant TR (b) was used for both simulations and measurements. TR1: minimal TR using short RF pulse durations; TR2: maximal TR using long RF pulse durations. In sequence scheme (a), prominent MT effects are expected to be present in the scheme using TR1, whereas signal modulation from MT is expected to be reduced in the scheme using TR2 as a result of RF pulse prolongation. In sequence scheme (b), prominent MT effects are expected to be present in the scheme using RF1, whereas signal modulation from MT is expected to be reduced in the scheme using RF2.

less than 20 Hz were achieved within the brain by manual shimming). For T_1 calculation, two three-dimensional SPGR datasets were acquired with a set to 3° and 17° ; isotropic resolution of 2.0 mm; matrix size of $64 \times 64 \times 72$ for the phantom, and $128 \times 128 \times 88$ for the volunteer; and TR was set to 9.8 ms. The T_1 map was then generated according to the DESPOT1 method (17,18). The three-dimensional bSSFP sequence was set up with a range of parameters fixed for all scans: TR was fixed to 4.78 ms, echo time to a typical $TR/2 = 2.39 \text{ ms}$, a matrix size of $64 \times 64 \times 72$ for the phantom and $128 \times 128 \times 88$ for the volunteer, and a 2.0 mm isotropic resolution. For each T_2 calculation by the DESPOT2 method (18), T_1 from the DESPOT1 method was used combined with two three-dimensional bSSFP datasets with different flip angles ($\alpha = 15^\circ$ and 55°). T_{RF} is varied: for rectangular pulses, $T_{RF} = 140, 300, 600, 1400, \text{ and } 1900 \text{ ms}$, while for the sinc pulses (time bandwidth = 2.7), $T_{RF} = 320, 600, 900, 1500, \text{ and } 1900 \text{ ms}$. Minimal T_{RF} settings were limited by specific absorption rate (SAR) restrictions (rectangular pulses with $T_{RF} = 140 \text{ ms}$ and sinc pulses with $T_{RF} = 320 \text{ ms}$, both with $\alpha = 55^\circ$, could therefore only be applied to the phantom). To preserve TR while reducing T_{RF} , a symmetrical delay was implemented in the sequence to keep echo time at $TR/2$ (Fig. 1).

For comparison of the results, averaged signal intensity within several regions of interest (ROIs) was used: a circular ROI is drawn on a central slice of the phantom data and three ROIs are drawn in

the volunteer data (cerebrospinal fluid (CSF), frontal white matter, and caudate nucleus, top row of Fig. 3), all in the 17° three-dimensional SPGR dataset. Signal deviation ($\Delta S = 100 (S(T_{RF}) - S(T_{RF} = 1900 \mu s)) / S(T_{RF} = 1900 \mu s))$) is calculated relative to the near MT-free signal (using $T_{RF} = 1900 \mu s$), i.e., within the limit of long RF pulses. Within this limit, the bSSFP signal should follow the Freeman-Hill formulae, and therefore T_2 estimation using the DESPOT2 method should be appropriate. Therefore, deviations in T_2 ($\Delta T_2 = 100 (T_2(T_{RF}) - T_2(T_{RF} = 1900 \mu s)) / T_2(T_{RF} = 1900 \mu s))$) are given relative to the T_2 obtained from the near MT-free signals.

To investigate the dependency of the found ΔT_2 on MT effects, scatterplots of the found ΔT_2 versus the MTR ($MTR = (S(T_{RF} = 1900 \mu s) - S(T_{RF})) / S(T_{RF} = 1900 \mu s))$) are generated. A Pearson's r^2 value is calculated, indicating the attribution of variance in the MTR to the variance in ΔT_2 .

RESULTS

First, results of the simulations will be shown, followed by those of the experiments.

Numerical Simulations

Numerical simulations show a clear effect of MT on the signal intensity and T_2 . Results are shown in Fig. 2, down to $T_{RF} = 140 \mu\text{s}$. As expected, less

MT-related signal variation is observed with lower flip angles. The signal increases with longer T_{RF} and therefore approaches to the Freeman-Hill formulae, where the DESPOT2 estimation should be correct. The resulting difference between the signal dependency on T_{RF} between low and high flip angle also decreases with increasing T_{RF} . This difference ($S(T_{RF}, \alpha_{\text{low}}) - S(T_{RF}, \alpha_{\text{high}})$) is responsible for the variations in the T_2 estimate. There is one

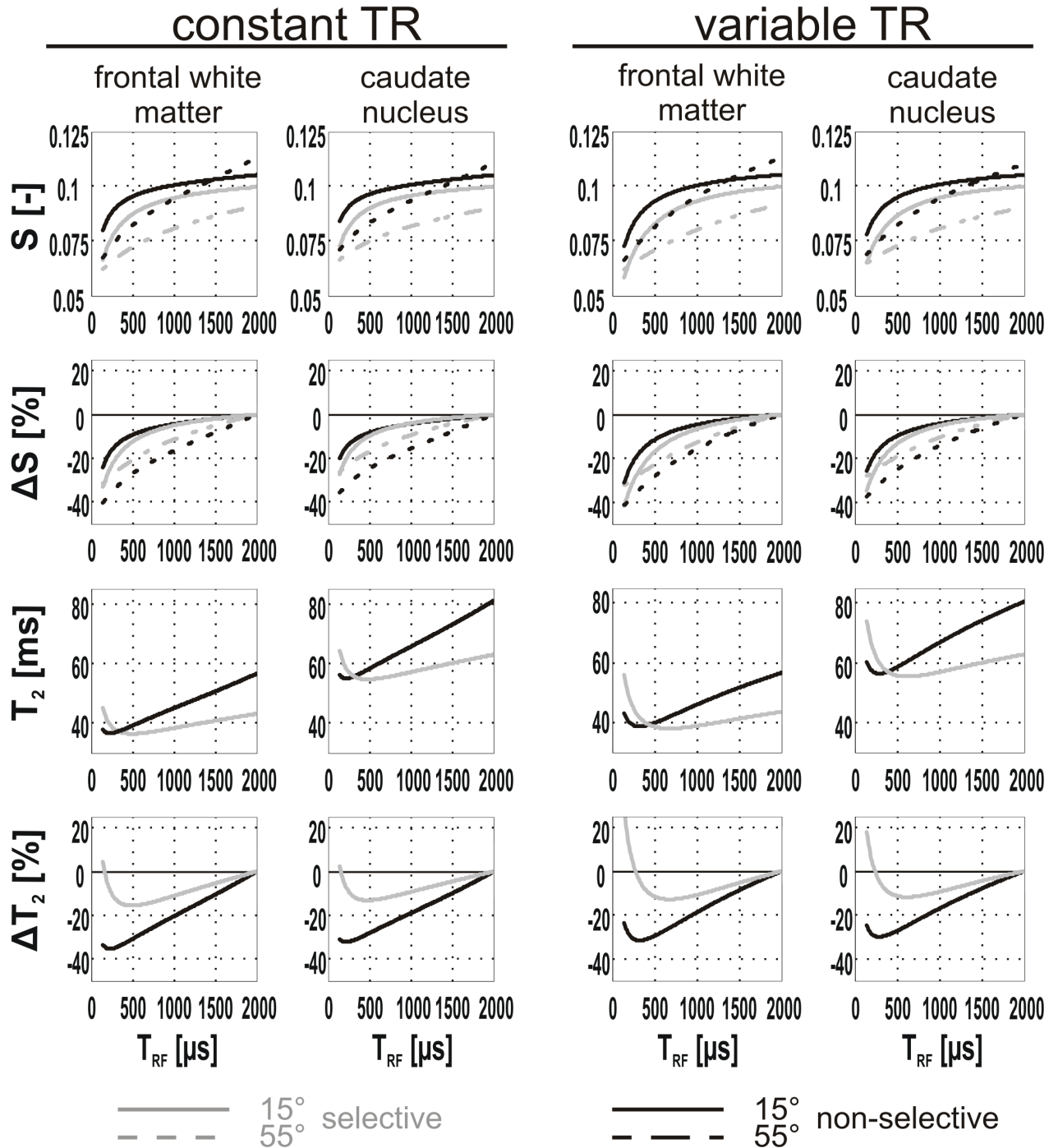


Figure 2. Results of the numerical simulation with constant TR (left) and variable TR (right), each for both frontal white matter and the caudate nucleus. From top to bottom (all as a function of T_{RF}): signal intensity, relative signal intensity deviation, calculated T_2 , and relative calculated T_2 deviation. Signal intensity results (graphs in top two rows) of rectangular excitation pulses with 15° and 55° flip angles are indicated by a continuous black line and a dotted black line, respectively; sinc pulse excitation with 15° and 55° flip angles are indicated by a continuous gray line and a dash-dot gray line, respectively. T_2 results of the rectangular excitation pulses are indicated with a black line, while the sinc pulse results are indicated with a gray one (graphs in the bottom two rows).

Table 1. Deviation percentages as observed in the numerical simulations for the signal intensities and the determined T_2 relaxation times at the minimal T_{RF} used on the volunteer (300 μ s and 600 μ s for the non-selective and selective RF excitation pulses, respectively).

	constant TR		variable TR	
	frontal white matter	caudate nucleus	frontal white matter	caudate nucleus
15° non-sel. pulse	-14,0%	-12,1%	-18,3%	-15,2%
15° sel. pulse	-10,2%	-8,0%	-13,9%	-10,8%
55° non-sel. pulse	-33,2%	-29,8%	-34,8%	-31,4%
55° sel. pulse	-18,5%	-15,1%	-20,5%	-17,2%
T_2 non-sel. pulse	-34,6%	-31,5%	-31,6%	-30,0%
T_2 sel. pulse	-15,2%	-12,7%	-12,7%	-11,9%

unique short T_{RF} value found for every simulation that results in a T_2 value equal to the T_2 found using long T_{RF} ($\Delta T_2 = 0$; i.e., in Fig. 2 it is seen that delta T_2 crosses 0 for one unique short T_{RF} value, while for long T_{RF} the found T_2 value approaches a steady state); however, this is a pure theoretical finding and is practically not feasible.

Calculated T_2 deviations at the minimal T_{RF} used on the volunteer (300 μ s for rectangular pulses and 600 μ s for sinc pulses) are shown in Table 1 for comparison with the experimental results for the same settings in Table 2. Further, it is observed that the difference between a variable and constant TR is always less than 4.5%.

Numerical simulations performed for MT-free cases result in a constant T_2 value for all T_{RF} and TR variations, and therefore 0% deviation in T_2 (ΔT_2) is observed (results are not shown).

Experiments

Using DESPOT1, T_1 is 150 ms for the phantom, 12 sec for CSF, 680 ms for frontal white matter, and 1140 ms for the caudate nucleus, which is in accordance to literature where for white and gray matter values of 591-884 ms and 998-1404 ms are

found, respectively (19,20). The flip angles for the DESPOT1 method were chosen to be optimal for tissues. As a result, the observed high T_1 value of CSF is most likely a result of suboptimal flip angle settings for CSF. The bSSFP signal as a function of T_{RF} varies only little for both the phantom and the CSF ROIs (as shown in Fig. 3 and Table 2), indicating that these ROIs are (almost) MT free. This is also indicated by the small difference between the small and large flip angle measurements. Although there is only a small difference in signal intensity between the two flip angles and the signal intensity dependency on T_{RF} is opposite to the dependency in the case of MT effect, the T_2 estimation based on these measurements shows an MT-like deviation.

For the frontal white matter and the caudate nucleus, the signal intensity decreases with decreasing T_{RF} , indicating MT effect. This is also shown in the resulting T_2 estimations based on these signal intensities (Fig. 3). However, the observed deviation in estimated T_2 is larger than predicted by the simulations (Tables 1 and 2). The maximal deviations observed are shown in Table 2, where it is seen that T_2 is underestimated for every ROI and also

Table 2. Deviation percentages for both signal intensity and T_2 per ROI at the minimal T_{RF} used on the volunteer (300 μ s and 600 μ s for the non-selective and selective RF excitation pulses, respectively) as observed in the measurements.

	phantom	CSF	frontal white matter	caudate nucleus
15° non-sel. pulse	8,0%	5,0%	-19,0%	-16,0%
15° sel. pulse	5,0%	7,0%	-12,0%	-11,0%
55° non-sel. pulse	3,0%	-2,0%	-43,0%	-37,0%
55° sel. pulse	2,0%	< 1%	-25,0%	-23,0%
T_2 non-sel. pulse	-22,0%	-17,0%	-53,0%	-46,0%
T_2 sel. pulse	-15,0%	-20,0%	-36,0%	-29,0%

for those where no MT effect is present (phantom and CSF) when short T_{RF} is used.

In the limit of sufficiently long RF pulses ($T_{RF} \rightarrow 2000 \mu\text{s}$ for rectangular pulses), the simple one-pool model is restored, which allows for proper

T_2 estimation by DESPOT2: phantom $T_2 = 153 \mu\text{s}$ (monoexponential fit through multicontrast spin-echo dataset: $T_2 = 120 \text{ ms}$); white and gray matter, 72 ms and 87 ms, respectively (literature reports T_2 values for white matter of 69-98 ms and for gray

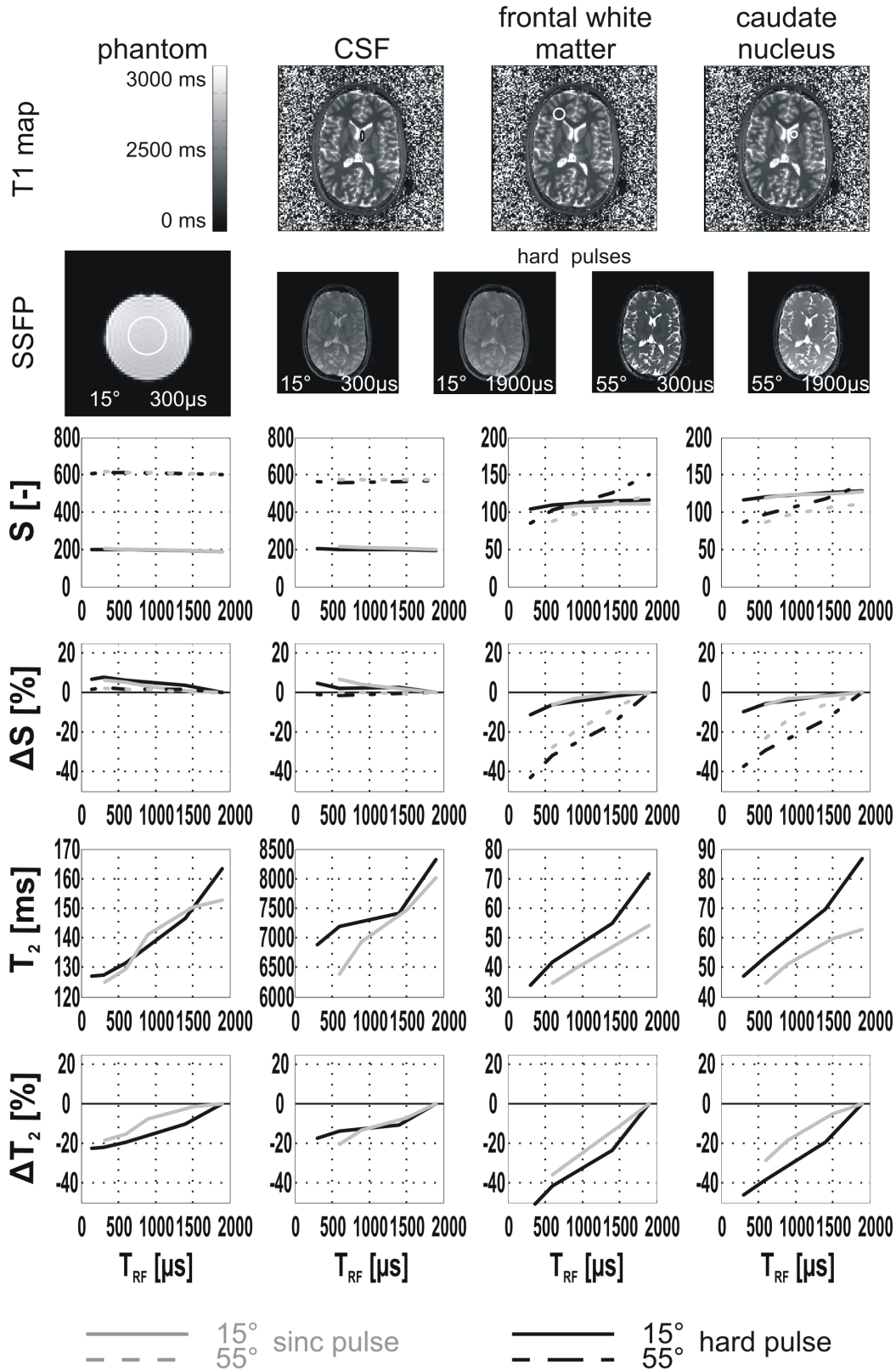


Figure 3. Measurement results with constant TR for ROIs, as indicated on the top row (from left to right: phantom, CSF, frontal white matter, and caudate nucleus). Graphs show from top to bottom (all as a function of T_{RF}): signal intensity, relative signal intensity deviation, calculated T_2 , and relative calculated T_2 deviation. Signal intensity results (graphs in top two rows) of rectangular excitation pulses with 15° and 55° flip angles are indicated by a continuous black line and a dotted black line, respectively; sinc pulse excitation with 15° and 55° flip angles are indicated by a continuous gray line and a dash-dot gray line, respectively. T_2 results of the rectangular pulse excitation are indicated with a black line, while the sinc pulse results are indicated with a gray one (graphs in bottom two rows).

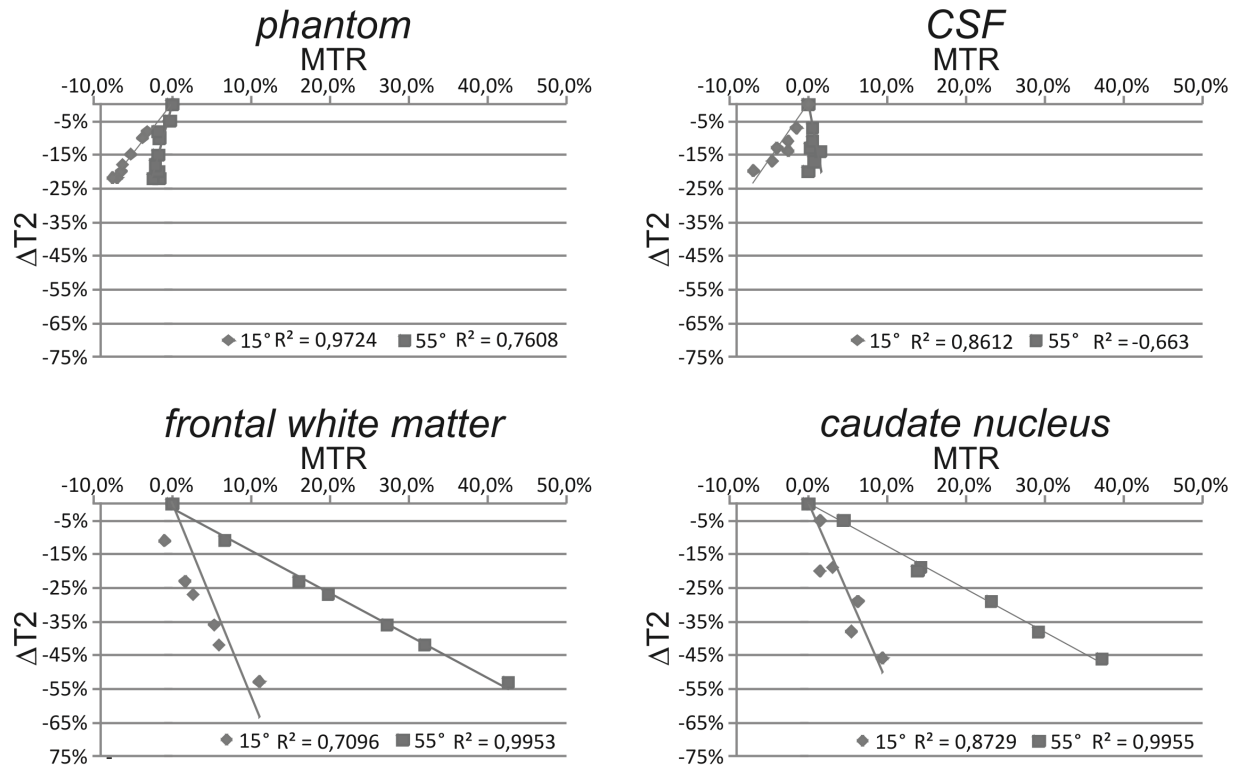


Figure 4. Scatterplot of the T_2 difference (ΔT_2) versus the MTR. Results are shown for all measurements performed and shown in Fig. 3 both for the 15° flip angle (diamonds) and the 55° flip angle (squares). Linear trend lines are plotted for each data series and the R^2 values shown in the legend. From left to right and top to bottom, data are shown for the phantom, the CSF, the frontal white matter, and the caudate nucleus. All correlations are found to be large ($R^2 > 0.5$), indicating a clear relation between the MTR and the ΔT_2 .

matter of 78-116 ms (19,20)). The T_2 estimation for CSF is incorrect, which can be related to the T_1 found and used as an input (12 sec, where literature describes values from 4-5 sec (21)). For the sinc pulses, the limit of sufficiently long pulses is not yet reached at $T_{RF} \rightarrow 2000 \mu\text{s}$ due to the time-bandwidth product of 2.7; this will only be the case at longer pulse durations.

The Pearson's r^2 values indicate large correlation ($R^2 > 0.5$) between the ΔT_2 and the MTR for all four ROIs drawn both in the phantom and the volunteer data (Fig. 4).

DISCUSSION

According to the Freeman-Hill formulae, no signal change with RF pulse modulation (TR modulation) is expected for aqueous probes. Nevertheless, a slight increase in both the CSF and the phantom signal with decreasing RF pulse duration was observed ($\Delta S = 5\text{-}7\%$; $\alpha = 15^\circ$), but only for low excitation angles ($\Delta S = 1\text{-}2\%$; $\alpha = 55^\circ$).

Both CSF and phantom measurements show deviation in T_2 in a similar way as MT effect (larger underestimation with shorter pulse duration), while it is expected that in absence of MT no change in observed T_2 would take place. Several short tests excluded that this observed signal behavior is caused by eddy currents (by changing the gradient amplitude and rise times): different delay times with different T_{RF} (very long delay to make delay difference minimal compared to the total delay time), the delay itself (delay versus no delay case (see also simulation results)), and flip angle imperfection (single excitation and readout for a range of RF pulse durations with equal flip angle).

In the ROIs with MT effect, it is shown that the deviation of T_2 is larger than expected, as given by the numerical simulations. However, when taking into account the deviation observed in both the phantom and the CSF, and subtracting this deviation, it is found that this corrected deviation is within the range of the simulations.

The lowest T_{RF} values used in the numerical simulations could not be tested on a volunteer due to SAR limitations. Therefore, it could not be tested if this part of the behavior is similar in a volunteer, as is predicted by the simulations.

The DESPOT2 method performed with a range of T_{RF} values on a phantom and CSF, both ROIs MT free, shows a clear deviation in obtained T_2 . After excluding all other possibilities, this can only be caused by scanner imperfection. The method can nevertheless be used to get an idea of T_2 values of samples and MT-free tissue when a deviation up to 22% (underestimation) relative to the T_2 obtained with a $T_{RF} = 1900 \mu\text{s}$ is acceptable.

The minimal TR setting is 3 ms ($T_{RF} = 300 \mu\text{s}$), which is elongated to a TR of 5.6 ms ($T_{RF} = 1900 \mu\text{s}$). This is a scan-time efficiency reduction of 53% for the bSSFP acquisition. However, the DESPOT2 method needs the DESPOT1 method, which has a typical TR of around 10 ms (22). The overall scan-time efficiency reduction therefore becomes 12%.

CONCLUSIONS

Both numerical simulation and measurements confirmed the influence of the MT effect on the derived T_2 values, using DESPOT2. Larger flip angles and shorter RF pulses result in larger signal changes due to MT. Within the limit of sufficiently long RF pulses in order to suppress MT related signal modulations allows for proper T_2 estimation with variable nutation SSFP. Due to the suggested elongation of the RF pulse duration in the bSSFP acquisition, the overall scan-time efficiency for the DESPOT2 method is reduced marginally (approximately 10%).

REFERENCES

1. Schmitt P, Griswold MA, Jakob PM, Kotas M, Gulani V, Flentje M, Haase A. Inversion recovery TrueFISP: quantification of T_1 , T_2 , and spin density *Magn Reson Med* 2004;51:661–667.
2. Deoni SC, Rutt BK, Peters TM. Rapid combined T_1 and T_2 mapping using gradient recalled acquisition in the steady state. *Magn Reson Med* 2003;49:515–526.
3. Oppelt A, Graumann R, Barfuss H, Fischer H, Hartl W, Schajor W. FISP: eine neue schnelle Pulssequenz für die Kernspintomographie. *Electromedia* 1986;54:15–18.
4. Christensen KA, Grand DM, Schulman EM, Walling C. Optimal determination of relaxation times of Fourier transform nuclear magnetic resonance: determination of spin-lattice relaxation times in chemically polarized species. *J Phys Chem* 1974;78:1971–1977.
5. Deoni SC, Ward HA, Peters TM, Rutt BK. Rapid T_2 estimation with phase-cycled variable nutation steady-state free precession. *Magn Reson Med* 2004;52:435–439.
6. Freeman R, Hill H. Phase and intensity anomalies in Fourier transform NMR. *J Magn Reson* 1971;14:366–383.
7. Haacke E, Brown R, Thompson M, Venkatesan R. Magnetic resonance imaging: physical principles and sequence design. New York: Wiley; 1999. pp 451–482.
8. Bieri O, Scheffler K. On the origin of apparent low tissue signals in balanced SSFP. *Magn Reson Med* 2006;56:1067–1074.
9. Wolff SD, Balaban RS. Magnetization transfer contrast (MTC) and tissue water proton relaxation in vivo. *Magn Reson Med* 1989;10:135–144.
10. Zu Z, Yu Y, Iiu Q, Zhao X, Chen M, Bao S. Magnetization transfer effect on T_2 measurement using steady-state free precession. *ISMRM*, Toronto, Ontario, Canada: 2008;1415.
11. Ou X, Gochberg DF. MT effects and T_1 quantification in singleslice spoiled gradient echo imaging. *Magn Reson Med* 2008;59:835–845.
12. Bieri O, Scheffler K. Optimized balanced steady-state free precession magnetization transfer imaging. *Magn Reson Med* 2007;58:511–518.
13. Henkelman RM, Huang X, Xiang QS, Stanisz GJ, Swanson SD, Bronskill MJ. Quantitative interpretation of magnetization transfer. *Magn Reson Med* 1993;29:759–766.
14. Sled JG, Pike GB. Quantitative imaging of magnetization transfer exchange and relaxation properties in vivo using MRI. *Magn Reson Med* 2001;46:923–931.
15. Gloor M, Scheffler K, Bieri O. Quantitative magnetization transfer imaging using balanced SSFP. *Magn Reson Med* 2008;60:691–700.
16. Morrison C, Henkelman RM. A model for magnetization transfer in tissues. *Magn Reson Med* 1995;33:475–482.
17. Homer J, Roberts JK. Conditions for the driven equilibrium single pulse observation of spin-lattice relaxation times. *J Magn Reson* 1987;53:424–432.
18. Deoni SC, Peters TM, Rutt BK. High-resolution T_1 and T_2 mapping of the brain in a clinically acceptable time with DESPOT1 and DESPOT2. *Magn Reson Med* 2005;53:237–241.
19. Aubert-Broche B, Grova C, Pike GB, Collins DL. Clustering of atlasdefined cortical regions based on relaxation times and proton density. *Neuroimage* 2009;47:523–532.
20. Stanisz GJ, Odobina EE, Pun J, Escaravage M, Graham SJ, Bronskill MJ, Henkelman RM. T_1 , T_2 relaxation and magnetization transfer in tissue at 3T. *Magn Reson Med* 2005;54:507–512.
21. Rooney WD, Johnson G, Li X, Cohen ER, Kim SG, Ugurbil K, Springer CS Jr. Magnetic field and tissue dependencies of human brain longitudinal 1H₂O relaxation in vivo. *Magn Reson Med* 2007;57:308–318.
22. Deoni SC, Williams SC, Jezzard P, Suckling J, Murphy DG, Jones DK. Standardized structural magnetic resonance imaging in multicentre studies using quantitative T_1 and T_2 imaging at 1.5 T. *Neuroimage* 2008;40:662–671.

3

Finite RF Pulse Correction on DESPOT2

Magnetization transfer and finite radiofrequency (RF) pulses affect the steady state of balanced steady state free precession. As quantification of transverse relaxation (T_2) with driven equilibrium single pulse observation of T_2 is based on two balanced steady state free precession acquisitions, both effects can influence the outcome of this method: a short RF pulse per repetition time ($T_{RF}/TR \ll 1$) leads to considerable magnetization transfer effects, whereas prolonged RF pulses ($T_{RF}/TR > 0.2$) minimize magnetization transfer effects, but lead to increased finite pulse effects. A correction for finite pulse effects is thus implemented in the driven equilibrium single pulse observation of T_2 theory to compensate for reduced transverse relaxation effects during excitation. It is shown that the correction successfully removes the driven equilibrium single pulse observation of T_2 dependency on the RF pulse duration. A reduction of the variation in obtained T_2 from over 50% to less than 10% is achieved. We hereby provide a means of acquiring magnetization transfer-free balanced steady state free precession images to yield accurate T_2 values using elongated RF pulses.

An adapted version of this chapter has been published as: H.J.A. Crooijmans, K. Scheffler, and O. Bieri. Finite RF Pulse Correction on DESPOT2. *Magn Reson Med*, 65(3):858-862, 2010

INTRODUCTION

Driven equilibrium single pulse observation of T_2 (DESPOT2) is a fast and efficient method of acquiring transverse relaxation time (T_2) maps on a voxel-wise basis with high resolution in a clinically acceptable time (down to less than 1 mm³ isotropic is possible in less than 30 minutes) (1). The DESPOT2 method is based on (i) two RF spoiled gradient echo (SPGR) and (ii) two balanced steady state free precession (bSSFP) acquisitions (2). The longitudinal relaxation time (T_1) needs to be calculated first from the two RF spoiled gradient echo acquisitions with constant pulse repetition time (TR) and varied flip angle (α) through a linearization of the SPGR signal equation (3). This T_1 and the two bSSFP acquisitions, also acquired with constant TR and varied α , are then used to calculate T_2 through a similar linearization of the Freeman-Hill equation (4). Maximized estimate precision is achieved by a flip angle choice as described by (5), and can be achieved for both T_1 and T_2 .

Only recently, however, it was realized that magnetization transfer (MT) effects, inherent to all SSFP type of sequences, can have a considerable impact on the estimate precision and accuracy of the DESPOT2 method (6) and generally lead to an underestimation in T_2 in tissues that show prominent MT effects, such as brain, muscle, liver and many others. As a result, the use of long RF pulses (1 ms) with DESPOT2 was suggested (6), since MT effects can be modulated by a simple RF pulse elongation scheme (7). Thus, in principle, the use of long RF pulses is capable of solving MT-related issues in SSFP, but only recently considerable deviations from the common bSSFP signal description were observed with finite RF pulses (8). The influence of finite pulse effects on the signal intensity is larger in cases of larger flip angles (8), which implies different finite pulse effects for the different bSSFP acquisitions used in the DESPOT2 method. Because of this difference between the signal changes in both acquisitions, an effect on the outcome of the DESPOT2 method is expected.

In this work, a correction for finite pulse effects (8) is implemented in the DESPOT2 theory, compensating for the relaxation during excitation, and therefore removing the DESPOT2 dependency on RF pulse duration. This implementation enables the use of MT-free bSSFP acquisition to acquire accurate T_2 values, which is proven by simulations as well as measurements.

METHODS

All numerical simulations, data analysis and visualizations were performed using Matlab R2007b (The MathWorks, Natick, MA).

DESPOT2 with Finite RF Pulses

In the derivation of the common SSFP signal theory, quasi-instantaneous acting RF pulses are assumed and it has been shown that finite RF pulses can lead to considerable deviations between signal measurements and theoretical predictions from an overestimation of transverse relaxation effects during the action of the RF pulse (8): No T_2 relaxation takes place during the fractional RF pulse duration

$$\zeta^{T_{RFE}} \approx \begin{pmatrix} 0.68 - \dots \\ 0.125(1 + T_{RFE}/TR)T_2/T_1 \end{pmatrix} \quad [1]$$

where T_{RFE} is the duration of a hard pulse equivalent calculated from an arbitrary RF pulse envelope, compare Eq. 11 and Eq. A.9 in (8). For hard pulses of duration T_{RF} it is given by

$$T_{RFE} = T_{RF} \quad [2]$$

From this, finite RF pulse effects can be corrected in the T_2 formula of the DESPOT2 method, from a simple substitution of $TR \rightarrow TR - \zeta T_{RFE}$ to yield

$$T_2 = \frac{-(TR - 0.68T_{RFE})}{\left(\ln \left(\frac{m - E_1}{mE_1 - 1} \right) + \dots \right)} \quad [3]$$

$$\left(0.125 \left(1 + \frac{T_{RFE}}{TR} \right) \frac{T_{RFE}}{T_1} \right)$$

Here, $E_1 := e^{-TR/T_1}$ is not modified, since to first order only transverse magnetization components are affected by finite pulse effects and m is the slope of the linear form of the signal equation used for the DESPOT2 method, as described in detail in (1), defined as:

$$m \equiv \frac{S_2/\sin \alpha_2 - S_1/\sin \alpha_1}{S_2/\tan \alpha_2 - S_1/\tan \alpha_1} \quad [4]$$

where $S_{1,2}$ and $\alpha_{1,2}$ refer to the signal and flip angle of the first and second bSSFP scan, respectively. For instantaneous pulses (i.e., $T_{RFE} = 0$), Eq. 3 simplifies to the common DESPOT2 equation as initially introduced by Deoni et al. in (1).

Two-Pool Bloch Simulation

The MT effect can be modeled by a two-pool model (a.k.a. binary spin-bath model) as described in detail elsewhere (9–12). In contrast to common MT prepared SPGR methods, the RF pulse train used for imaging is responsible for the MT effect with bSSFP.

A standard solver (“ode45” function) was used to solve the system of differential equations for two pool modeling of MT effects with bSSFP using alternating phase ($\pm\alpha$) as described in detail in reference (11). For this model, several parameters have to be set: the various spatial components (x, y, and z) of the magnetization vector \mathbf{M} ; the longitudinal relaxation rate $R_{1,f}$ (with $R_{1,r} = R_{1,f}$), and the transversal relaxation rate $R_{2,f}$ ($R_{2,r}$) of the free (restricted) pool; the magnetization exchange is given by the pseudo-first-order rate constants $k_f = RM_{o,r}$ and $k_r = RM_{o,f}$ with R the fundamental rate constant between the two pools; the equilibrium magnetization of the free (restricted) pool $M_{o,f}$ ($M_{o,r}$); and the fractional size of the restricted pool amounts $F := M_{o,r}/M_{o,f}$ and thus $k_r = k_f/F$. The effect of pulsed radiation (13) on the longitudinal magnetization of the restricted pool protons is described by the mean saturation rate $W(\Delta)$. Two-pool model simulation parameters for gray and white matter are listed in Table 1.

The simulation was ended after 1000 iterations and the signal was read at a signal readout block at echo time $TE = TR/2$ within iteration 1000. The RF pulse amplitude (A) was defined to achieve the desired flip angle in the limit of infinitesimal excitation pulses ($T_{RF} \rightarrow 0$, $A \rightarrow 8$), i.e., using

Table 1. Parameter settings as used in the Bloch simulations.

Tissue Model	$W(\text{s}^{-1})$	$M_{o,f}(-)$	gray matter				white matter			
			$T_{1,f}(\text{ms})$	$T_{2,f}(\text{ms})$	$F(-)$	$k_f(\text{s}^{-1})$	$T_{1,f}(\text{ms})$	$T_{2,f}(\text{ms})$	$F(-)$	$k_f(\text{s}^{-1})$
single pool	-	-	1087	59	-	-	733	40	-	-
2 pool no MT	0	1	1087	59	0.065	2.3	733	40	0.145	4.5
2 pool MT	$W(\Delta \rightarrow 0)$	1	1087	59	0.065	2.3	733	40	0.145	4.5

$T_{RF} = 1 \mu\text{s}$ ($\rightarrow A_0$), and was linearly decreased ($A = 1/\beta \cdot A_0$) with increasing RF pulse duration ($T_{RF} = \beta \cdot 1 \mu\text{s}$, prolongation by a factor β). A TR of 8 ms was chosen for the simulations. The RF pulse duration was varied between $0 < T_{RF} < TR$ and therefore finite RF pulse effects are naturally included in the Bloch simulations. Thus, in general, two-pool model simulations show contributions from both, MT and finite RF pulse effects. But, whereas finite RF pulse effects increase with increasing RF pulse duration, MT effects decrease. Therefore, we determined the T_{RF}/TR ratio above which the finite pulse effect dominates over the MT effect (simulation parameter settings are shown in Table 1). The influence of the MT effect is calculated as the difference between two simulations, one with and one without saturation of the restricted pool fraction ($W(\Delta \rightarrow 0)$ and $W = 0$, respectively), whereas the finite RF pulse effect is defined by the deviation of the signal intensity from the signal intensity at $T_{RF} \rightarrow 0$ without MT.

Single-Pool Bloch Simulation

The implementation of the finite pulse effect correction in the DESPOT2 method needs to be tested for effectiveness and correctness first on a simple one-pool model since the Freeman-Hill formulae used in the DESPOT2 theory assumes a single pool situation, .i.e., no MT effects. For this, the two-pool model is reduced to a single-pool model by setting the exchange rate R to zero. The corrected DESPOT2 formula (Eq. 3) is compared to the original DESPOT2 method ($T_{RFE} = 0$ in Eq. 3) on the same input data for both gray and white matter (simulation parameter settings are given in Table 1).

Measurements

Measurements were performed on a spherical phantom (64 mm diameter, 1 mM gadolinium in water) and a healthy volunteer on a 1.5 T Espree whole body scanner (Siemens Healthcare, Erlangen, Germany). Images covering the whole phantom (128x64x72 matrix) and whole brain images (192x192x144 matrix) both with an isotropic resolution of 1.3x1.3x1.3 mm³ were acquired. Two 3D SPGR acquisitions were performed ($TR = 9.8$ ms; $TE = 4.3$ ms; $\alpha_{1,2} = 4^\circ, 15^\circ$) to calculate the T_1 by the DESPOT1 method (1). These acquisitions were followed by a series of two alternating phase ($\pm\alpha$) bSSFP acquisitions ($TR = 8$ ms; $TE = TR/2$; $\alpha_{1,2} = 15^\circ, 55^\circ$; typically, frequency variations of less than 20 Hz were achieved within the scanned volume (phantom, brain) by manual shimming) with various T_{RF} settings rang-

ing from 520 to 4800 μs covering a T_{RF}/TR range of 0.065–0.6 (a symmetric delay before and after the excitation pulse was used to preserve a constant TR , readout bandwidth and gradient timing amongst the series of acquisitions). These sets of two acquisitions with different flip angles are used to perform the DESPOT2 calculations, both with and without the correction for finite pulses. In addition, multiecho spin echo (mSE) images were acquired with 2x2 mm² in plane resolution (128x64 acquisition matrix) and 10 mm slice thickness for the phantom and single-echo spin echo (SE) images with 1.3x1.3 mm² in plane resolution (128x256 acquisition matrix) and 3 mm slice thickness for the brain. Finally, for comparison with the DESPOT2 outcome, T_2 values were derived from the mSE sequence ($TR = 3000$ ms; minimal $TE = 13.2$ ms; echo spacing 13.2 ms; 32 echoes (omitting the first echo for fit improvement)) using a mono-exponential least-squares fitting analysis (for the phantom) and from the (SE) sequence ($TR = 1100$ ms; $TE = 5, 6, 7, 9, 10, 12, 15, 18, 21, 25, 30, 36, 43, 51, 61, 73, 88, 105, 125, \text{ and } 150$ ms) using the same fitting procedure (for the human brain). Regions of interest (ROIs) for gray matter (caudate nucleus) and deep white matter were identified and selected from the sagittal 15° SPGR scan, for the phantom the central ROI is also selected in its 15° SPGR scan.

RESULTS

Finite Difference Simulations

The corrected finite pulse DESPOT2 equation is still prone to MT effects, since a one-pool situation is still assumed, similar to the original DESPOT2 equation. The accuracy of the proposed correction is thus first evaluated in the limit of vanishing MT effects (Fig. 1). It is seen that the correction reduces the dependency of the observed T_2 on T_{RF} drastically: For a practical limit of $T_{RF}/TR \sim 0.5$, an overestimation of about 50% in the T_2 by the uncorrected DESPOT2 method is observed, which reduces to less than 4% by implementation of the finite pulse correction. Furthermore, the derived T_2 values from the corrected DESPOT2 equation are virtually independent of the RF pulse duration and thus of finite RF pulse effects yielding accurate results for all systems showing one-pool signal behavior such as fluids. Tissues, however, in general show prominent MT effects and thus are better described by two-pool models.

Therefore, two-pool simulations for gray and white matter were performed. As expected, a clear influence of MT on the steady-state is observed, especially for very short RF pulses (see Figs. 2a and d). Generally, MT effects increase with decreasing RF pulse durations, whereas RF pulse effects increase

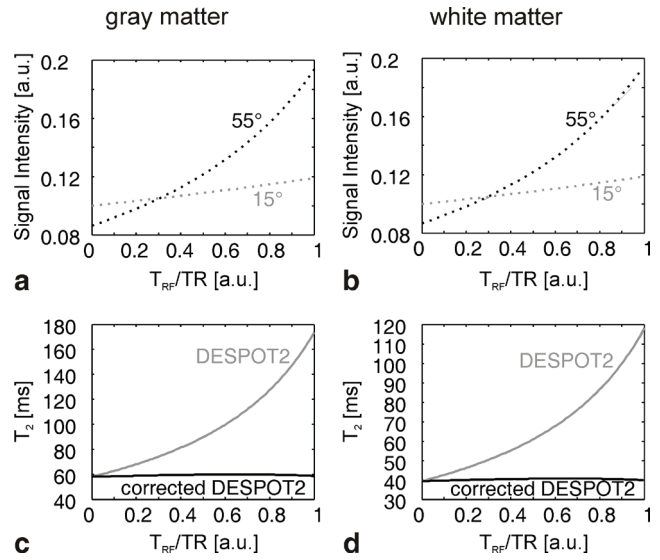


Figure 1. Results of the single pool Bloch simulation for gray and white matter (a and b, respectively): signal intensity as a function of T_{RF}/TR for both 15° and 55° flip angles. The T_2 values calculated from these signal intensities with the DESPOT2 and the corrected DESPOT2 method are shown in c and d for the gray and white matter, respectively. Single pool Bloch simulations do not include MT effects.

with increasing RF pulse durations. This raises the question: Which of the effects dominates at what RF pulse durations? To separate the two effects, also two-pool simulations were performed without the presence of MT effects (i.e., by setting W

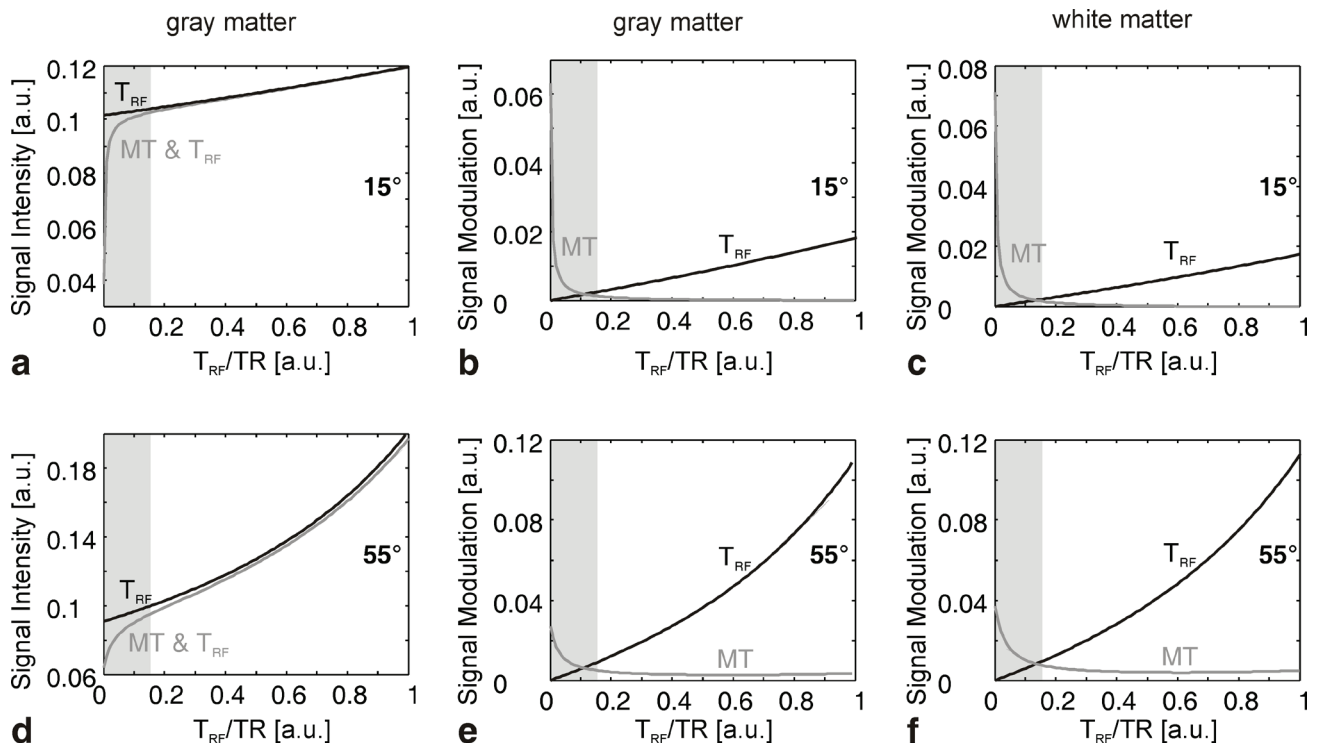


Figure 2. Results of the two-pool Bloch simulations for gray matter for a 15° and 55° flip angle (a and d, respectively). From a and d, the deviation due to the MT effect and the finite pulse effect (T_{RF}) are calculated and given in b and e, for the 15° and 55° flip angles, respectively. The same is done for white matter: the signal deviation for white matter is given in c and f for the 15° and 55° flip angle, respectively. All results are given as a function of T_{RF}/TR . The white graph area marks the range of T_{RF}/TR for which the finite pulse effect is dominant over the MT effect for both gray and white matter as well as both the 15° and 55° flip angle.

equal to zero). The pure MT effects are calculated from the difference between the outcomes of the two simulations; the finite RF pulse effect was defined by the deviation of the signal intensity from the signal intensity at $T_{RF}/TR \rightarrow 0$ (both from the simulation without MT). After separation of the MT and finite pulse effects, it is seen that the finite pulse effect dominates over the MT effect (for both 15° and 55° flip angles as well as for both gray and white matter) when $T_{RF}/TR > 0.15$ (see Figs. 2b, c, e, and f). For T_{RF}/TR values smaller than 0.15 the MT effect starts to dominate.

Measurements

The results for the experiments are given in Figure 3. For the phantom ROI (see Fig. 3a), signal intensities are shown as a function of T_{RF}/TR for $\alpha = 15^\circ$ and $\alpha = 55^\circ$ (Fig. 3c) and derived DESPOT2 values, both corrected and uncorrected, in combination with the mSE result ($T_2 = 120$ ms) are displayed in

Figure 3d. A maximum deviation of less than 8% in the derived T_2 values between the corrected DESPOT2 and the mSE T_2 is observed over the whole range of fractional T_{RF}/TR , whereas finite RF pulse effects lead to a nearly linear increase in the uncorrected DESPOT2 values with a maximum deviation of around 50% of the mSE derived T_2 .

In vivo results of signal intensities measured with a 15° and 55° flip angle in a gray and a white matter ROI (Fig. 3b) are shown in Figures 3d,e, and from these intensities calculated T_2 values are shown in Figures 3g, h. A clear increase in signal intensity is obtained with increasing T_{RF}/TR . The 55° flip angle shows a larger increase than the 15° flip angle, as expected according to the Bloch simulations (Figs. 1a and b, 2a and d) and theory (8). T_2 values calculated with the DESPOT2 method also show an increase with increasing T_{RF}/TR , which was also expected by the simulations (see Fig. 1). A reduction of this deviation by the implementation

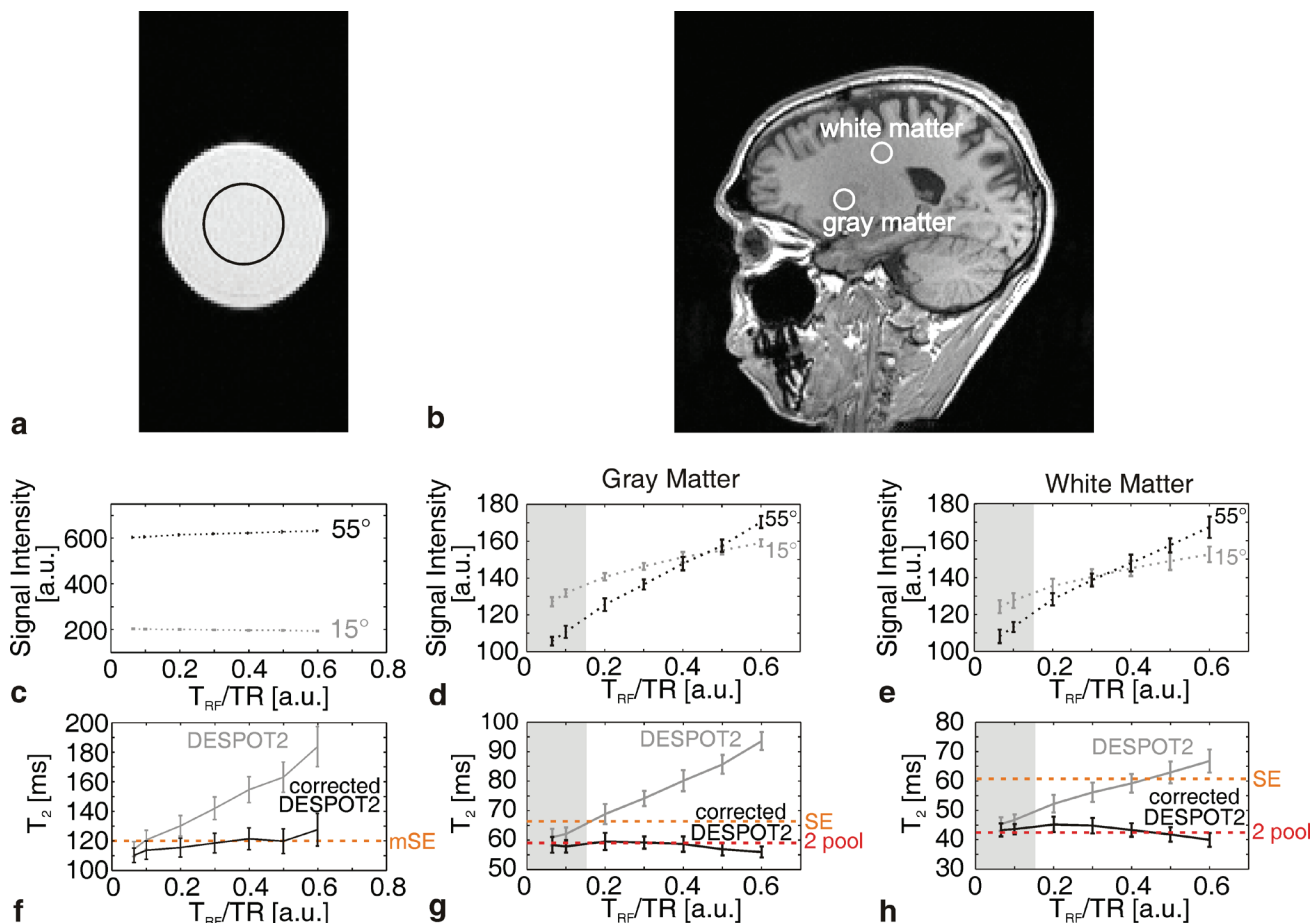


Figure 3. Measurement results for the phantom (64 mm diameter sphere filled with 1 mM gadolinium in water, **a**, **c**, and **f**) and for a healthy volunteer (**b**, **d**, **e**, **g**, and **h**). Data is shown for the ROIs as defined in **a** and **b**. For the phantom, the signal intensities for both 15° and 55° flip angle as a function of T_{RF}/TR (**c**) are used to calculate the T_2 values using the DESPOT2 and the corrected DESPOT2 method (**f**). In **f**, the T_2 value according to the multicontrast spin echo sequence is also shown. For the healthy volunteer's gray and white matter ROIs, the signal intensities for both 15° and 55° flip angle as a function of T_{RF}/TR (**d** and **e**) are used to calculate the T_2 values using the DESPOT2 and the corrected DESPOT2 method (**g** and **h**). The gray areas in **d**, **e**, **g**, and **h** indicate the region where the MT effect dominates over the finite pulse effect. In addition to the (corrected) DESPOT2 T_2 values, reference T_2 values are included in **g** and **h** according to the SE measurements as well as the two-pool model (caudate nucleus mSE $T_2 = 61$ ms; white matter mSE $T_2 = 66$ ms; T_2 values as presented in reference (11): caudate nucleus $T_2 = 59$ ms; white matter $T_2 = 45$ ms).

of the correction for finite pulse effects is achieved (Figs. 3g and h): for gray matter a reduction from 53% to 4% was achieved while a reduction from 48% to 10% was achieved in the white matter ROI (deviations relative to the T_2 at the shortest used T_{RF}/TR , which was 0.065). Although the dependency on the pulse duration is removed, a consistent underestimation of the T_2 compared to the SE T_2 value is obtained (caudate nucleus SE $T_2 = 66$ ms; white matter SE $T_2 = 61$ ms).

DISCUSSION AND CONCLUSIONS

Two main sources of signal deviations between measurements and theory for SSFP-type of sequences were recently identified: finite RF pulses (8) and MT effects (7). The influence of MT on the observed bSSFP signal can be reduced by RF pulse elongation and its impact on the derived T_2 from DESPOT2 is negligible for $T_{RFE}/TR > 0.15$. In this limit, however, the required substantial increase in the RF pulse duration gives rise to considerable finite RF pulse effects. Therefore, a simple correction of the linear form of the signal equation used for the DESPOT2 method (see Eq. 3) was derived to remove finite RF pulse effects. Although the shortest used T_{RFE}/TR ratio equals 0.065 which is below the 0.15 limit, only small influence of MT effect is expected (see also Fig. 2), and shown in Figure 3.

The phantom measurements (Fig. 3) indicate good correspondence between the corrected DESPOT2 and the mSE T_2 over the whole range of tested T_{RF}/TR values. However, for brain tissue a significant discrepancy is observed: the corrected DESPOT2 values systematically underestimate the apparent T_2 derived from SE measurements. Interestingly, for tissues, the corrected DESPOT2 value for gray and white matter levels off at the corresponding T_{2f} of the free pool protons (caudate nucleus $T_{2f} = 59$ ms; white matter $T_{2f} = 45$ ms) using a twopool bSSFP model analysis (9,11), indicating a different sequence specific weighting of the usually broad spectrum of T_2 values found in tissues.

In summary, it is proven that the finite pulse effect influences the outcome of the DESPOT2 method, and that this effect can be reduced from a deviation exceeding 50% to a marginal 10% deviation (% of the T_2 acquired at the shortest pulse duration ($T_{RF} = 520$ ms)) by the implementation of a correction factor. For a T_2 dispersion free phantom, the corrected DESPOT2 yields the same results as the standard mSE method. An underestimation compared to a SE T_2 is observed for tissues, however, the derived T_2 is comparable to that obtained by a two-pool model analysis (9,11). The implementation of the finite pulse correction factor does not lead to an elongation of calculation time, nor scan time and requires only one additional parameter (the effective pulse duration T_{RFE}) for finite pulse correction.

ACKNOWLEDGMENTS

The authors thank Monika Gloor for the implementation of the Bloch equations and her useful contribution to discussions according the use of these simulations. This work has been partially supported by NCCR CO-ME and SNF 325230-118377.

REFERENCES

1. Deoni SC, Rutt BK, Peters TM. Rapid combined T_1 and T_2 mapping using gradient recalled acquisition in the steady state. *Magn Reson Med* 2003;49:515–526.
2. Oppelt A, Graumann R, Barfuss H, Fischer H, Hartl W, Schajor W. FISP: eine neue schnelle Pulssequenz für die Kernspintomographie. *Electromedia* 1986;54:15–18.
3. Christensen KA, Grand DM, Schulman EM, Walling C. Optimal determination of relaxation times of Fourier transform nuclear magnetic resonance. Determination of spin-lattice relaxation times in chemically polarized species. *J Phys Chem* 1974;78:1971–1977.
4. Freeman R, Hill H. Phase and intensity anomalies in Fourier transform NMR. *J Magn Reson* 1971;14:366–383.
5. Deoni SC, Ward HA, Peters TM, Rutt BK. Rapid T_2 estimation with phase-cycled variable nutation steady-state free precession. *Magn Reson Med* 2004;52:435–439.
6. Crooijmans HJA, Bieri O, Scheffler K. Influence of MT effects on T_2 quantification with 3D balanced steady-state free precession imaging. *Magn Reson Med* 2010;65(1):195–201.
7. Bieri O, Scheffler K. Optimized balanced steady-state free precession magnetization transfer imaging. *Magn Reson Med* 2007;58:511–518.
8. Bieri O, Scheffler K. SSFP signal with finite RF pulses. *Magn Reson Med* 2009;62:1232–1241.
9. Sled JG, Pike GB. Quantitative imaging of magnetization transfer exchange and relaxation properties in vivo using MRI. *Magn Reson Med* 2001;46:923–931.
10. Morrison C, Henkelman RM. A model for magnetization transfer in tissues. *Magn Reson Med* 1995;33:475–482.
11. Gloor M, Scheffler K, Bieri O. Quantitative magnetization transfer imaging using balanced SSFP. *Magn Reson Med* 2008;60:691–700.
12. Ramani A, Dalton C, Miller DH, Tofts PS, Barker GJ. Precise estimate of fundamental in-vivo MT parameters in human brain in clinically feasible times. *Magn Reson Imaging* 2002;20:721–731.
13. Graham SJ, Henkelman RM. Understanding pulsed magnetization transfer. *J Magn Reson Imaging* 1997;7:903–912.

4

Single T_2 Acquisitions on a Multi- T_2 System

Although it is well known that brain tissue consists of exchanging multi T_2 compartments, it is still often measured with a single T_2 approach. Within this work, the spin-echo approach with mono-exponential T_2 decay fit and driven-equilibrium single-pulse observation of T_2 (DESPOT2) were compared for single T_2 acquisition on an coupled two compartment probe of which each had a measurable T_2 . Both simulation and measurement data have shown that the spin-echo observed T_2 in this case does not depend on the echo spacing. The DESPOT2 method has proven to underestimate T_2 compared to the spin echo approach by 15-18% of the spin-echo result in gray matter, and by 26-30% of the spin-echo result in white matter.

INTRODUCTION

It is known that brain tissue is a multi compartment system and exchange can take place between these compartments. Magnetization transfer (MT) is a very fast exchange between two pools of which the fast pool has a very short transversal relaxation time (T_2) value which is not measurable with clinical T_2 mapping protocols (1). However, the exchange between the free water protons and the protons of water trapped in between the myelin sheaths is between two pools with measurable T_2 values (1-3). Nevertheless, a single compartment assumption is commonly used in clinical T_2 mapping protocols (2-12).

Since it is known that the measured tissue in T_2 mapping of the brain consists of several compartments (13-16), it is commonly thought that the distribution of the echoes within a spin-echo experiment is crucial. For example, measuring two completely decoupled compartments with this approach, closer spacing will lead to a heavier weighting towards the compartment with shortest T_2 (fast compartment), and vice versa. This weighting can be further manipulated by the choice of unequally spaced echoes: logarithmically spaced echoes will lead to closer spacing in the short echo time (TE) region, resulting in a heavier weighting of the faster of the two compartments. All of the above is true for uncoupled compartments. However, the compartments within the brain tissue are coupled, exchange between the compartments takes place, and it becomes questionable whether or not the above is still valid for this case.

Recently, another T_2 mapping method has been developed: the driven-equilibrium single-pulse observation of T_2 (DESPOT2) method is a faster approach than the standard SE approach, and it only uses two acquisitions to obtain T_2 (with prior knowledge of T_1) (3,4). This method in principle also assesses a single compartment T_2 . Although it has been further developed to be able to assess multiple compartments (mcDESPOT2 (17)), the fastest approach is still a single compartment T_2 acquisition. DESPOT2 is based on balanced steady-state free-precession (bSSFP) acquisitions which are known to be MT sensitive (18) and this can affect the DESPOT2 outcome (19). To avoid influences of MT, long radio frequency (RF) excitation pulses are required. This might lead to finite pulse effect (20), which can be corrected for within the T_2 calculation of this method (21).

In order to keep the T_2 mapping within a

clinical acceptable time, multi-echo SE is a commonly used approach, acquiring several echoes within one pulse repetition time (TR). Limitations of this approach are the fixed echo spacing within this sequence, whereby the logarithmic spacing of echoes is no longer available and the occurrence of stimulated echoes. However, the SE is still considered the principle method in T_2 quantification.

Within this work, it is investigated how the exchanging multi compartment probe is influencing the outcome of a T_2 quantification method based on a single compartment assumption. The effect of the exchanging pools on a SE experiment can be dependent on the chosen echo spacing, as often thought. It is thus investigated how the choice of echo spacing and the number of echoes used for a mono-exponential fit changes the obtained T_2 of a coupled two pool system. Within the DESPOT2 method, TR and flip angles are the two parameters to be investigated. The choice of flip angles can be optimized (4), however, this is again for the assumption of a single T_1 - T_2 combination.

METHODS

Bloch simulations and data analysis were performed using Matlab R2007b (The MathWorks, Inc., Natick, MA). Measurements were performed on a 1.5 T Espree whole body scanner (Siemens Healthcare, Erlangen, Germany).

Modified Bloch equations

The Bloch equations were modified to include the exchange of magnetization between two compartments. The magnetization of the fast compartment (M^f , short T_1 and T_2) will decrease by $k_{fs}M^f$ and increase by $k_{sf}M^s$ if exchange between the compartments occurs (k_{fs} (k_{sf}) is the exchange rate from the fast to the slow compartment (slow to fast)). Similar to that, the magnetization of the slow compartment (M^s , long T_1 and T_2) will decrease by $k_{sf}M^s$ and increase by $k_{fs}M^f$. This leads to modified 6D Bloch equations (22), describing all spatial components of the two compartment magnetization vector $M = [M_x^f \ M_x^s \ M_y^f \ M_y^s \ M_z^f \ M_z^s]$:

$$\frac{dM_x^f}{dt} = \omega_0 M_y^f - \frac{M_x^f}{T_2^f} - k_{fs} M_x^f + k_{sf} M_x^s \quad [1]$$

$$\frac{dM_x^s}{dt} = \omega_0 M_y^s - \frac{M_x^s}{T_2^s} - k_{sf} M_x^s + k_{fs} M_x^f \quad [2]$$

$$\begin{aligned} \frac{dM_y^f}{dt} = \\ -\omega_0 M_x^f - \frac{M_y^f}{T_2^f} - k_{fs} M_y^f + k_{sf} M_y^s + \omega_1(t) M_z^f \end{aligned} \quad [3]$$

$$\begin{aligned} \frac{dM_y^s}{dt} = \\ -\omega_0 M_x^s - \frac{M_y^s}{T_2^s} - k_{sf} M_y^s + k_{fs} M_y^f + \omega_1(t) M_z^s \end{aligned} \quad [4]$$

$$\begin{aligned} \frac{dM_z^f}{dt} = \\ \frac{M_0^f - M_z^f}{T_1^f} - k_{fs} M_z^f + k_{sf} M_z^s - \omega_1(t) M_y^f \end{aligned} \quad [5]$$

$$\begin{aligned} \frac{dM_z^s}{dt} = \\ \frac{M_0^s - M_z^s}{T_1^s} - k_{sf} M_z^s + k_{fs} M_z^f - \omega_1(t) M_y^s \end{aligned} \quad [6]$$

Here, M_0^f (M_0^s) is the abbreviation for the equilibrium magnetization of the fast (slow) component, $\omega_0 = \gamma|B_1(t)|$. Moreover, it is assumed that $\omega_0 = \omega_0^f = \omega_0^s$. All simulations will be for the on resonance case, hence, $\omega_1(t) = 0$. These modified Bloch equations describe excitation, relaxation and exchange. $M_0^f = FM_0$ and $M_0^s = (1-F)M_0$, where F is the fractional size of the fast component. In kinetic equilibrium, the exchange rates k_{sf} and k_{fs} are related through the fractional sizes by $k_{fs} = (1/F-1)k_{sf}$. Further, the overall exchange rate k is defined as $k = k_{fs} + k_{sf}$, where $k_{fs} = Fk$ and $k_{sf} = (1-F)k$.

Signal intensity simulations and T_2 calculations

Signal intensities were simulated for tissue parameters of gray and white matter as found by Deoni et al. in (17) and given in Table 1. Simulations used instantaneous acting RF pulses, allowing for decoupling of the excitation from the relaxation and exchange within the simulations.

Table 1. Tissue parameter settings used in the two pool simulations for gray (Putamen) and white matter as obtained by Deoni et al. in reference (17).

parameter	unit	gray matter	white matter
T_1^s	s	1.100	0.900
T_2^s	s	0.110	0.120
T_1^f	s	0.500	0.400
T_2^f	s	0.013	0.014
F	-	0.10	0.28
k	s ⁻¹	10	10

Spin Echo

An ordinary differential equation solver (“ode45”) was used to solve the modified Bloch equations and calculate the signal decay of the SE sequence on a millisecond interval after the 90° excitation pulse, up to 500 ms. A selection of the calculated signal intensities was fitted mono-exponentially in order to acquire T_2 of the simulated tissue. The echo spacing was varied from 1 to 30 ms with a 1 ms increment, over the time spans 0 to 120 ms; 0 to 150 ms; and 0 to 300 ms. Hereby, the influence of the echo spacing on the fit result was investigated. Additionally, for the echo spacing of 5, 8 and 10 ms, the number of echoes was varied from 10 to 32 echoes to investigate the influence of the amount of echoes for these echo spacings on the obtained T_2 . Realistic time spans are never shorter than the observed T_2 .

RF spoiled gradient echo

Bloch simulations for 1000 spins over 200 iterations were performed to simulate the SPGR sequence. Each spin consisted of a fast and slow relaxing part simulating the two compartments. A solver for ordinary differential equations (“ode45”) was used to solve the modified Bloch equations. Gradient spoiling was simulated by distributing the spins over 2π at TR . The simulation was ran with a 4° and a 15° flip angle with a 50° RF spoiling increment; $TR = 9.8$ ms; $TE = 4.3$ ms. The average signal intensity at TE of the last 20 iterations was taken from both simulated flip angles to calculate T_1 according to the DESPOT1 approach. The used flip angles were optimized for maximal T_1 precision at the used TR (4), for $T_1 = 950$ ms.

Balanced SSFP

Single spin bSSFP Bloch simulations were performed over 1500 iterations to reach steady state for both the slow and fast part. Again, the same “ode45” solver was used to solve the modified Bloch equations. For investigation of both the flip angle and the TR settings on the outcome of the DESPOT2 method, flip angles between 0° and 90° were chosen in combination with $TR = 3.25$ ms and 10 ms.

Additionally, for the typical echo spacing of the SE (10 ms echo spacing, 32 echoes) (8,21), and the typical flip angle choice of DESPOT2 (15° and 55° , $TR = 3.25$ ms, $TE = TR/2$) (3,19,21), signal intensities were calculated for a range of $k = 0 - 15$ s⁻¹ and $F = 0 - 1$ using the T_1 and T_2 values of gray matter (Table 1).

Measurements

The simulations were verified by measurements on a phantom (single compartment system), and brain tissue (coupled multi-compartment system).

Spin Echo

$TR = 2.5$ s to ensure total recovery of the magnetization to its resting state within one TR . The signal was sampled with 25 echoes logarithmically spaced from 5 to 400 ms. These samples were interpolated to get a sample every millisecond for reconstruction of equally spaced echoes as done in the simulations to mimic multi echo spin echo acquisition echo spacing.

RF spoiled gradient echo

$TR = 9.8$ ms, $TE = 4.3$ ms and $\alpha_{1,2} = 4^\circ, 15^\circ$ with 50° RF spoiling increment.

Balanced SSFP

To avoid possible influences of the MT effect, $T_{RF} = 1600$ μ s (non-selective pulse) was used. The TR was set to the shortest possible value: $TR = 4.49$ ms; $TE = TR/2$; $\alpha_{1,2} = (15^\circ, 55^\circ), (20^\circ, 80^\circ)$.

Selections of the interpolated SE measurements were mono-exponentially fitted to determine T_2 . The SPGR and bSSFP datasets were processed with the DESPOT1 and DESPOT2 with finite pulse correction methods respectively. Both methods used the actual flip angles and signal intensities as input. The DESPOT2 additionally used the RF pulse duration and T_1 .

RESULTS

Simulations

The longer the time span over which the echoes were acquired, the larger the influence of the slow pool, i.e., the observed T_2 was larger when the echoes were distributed over a longer time span (Fig. 1a and b). It could additionally be observed that the above was clearer in the white matter data with a larger fast pool fraction than in the gray matter. A slight but insignificant increase in observed T_2 was seen with increased echo spacing (Fig. 1a, Table 2). In this experiment with fixed time spans, the increases of echo spacing (ΔTE) lead to a decrease of included echoes ($\#TE$). This increase was larger for white matter than for gray matter (i.e., larger standard deviations within one time span, Table 2). Nevertheless, the observed standard deviation never exceeded 4% of the mean observed T_2 (mean of the observed T_2 values of one time span) for the investigated range of echo times and time spans.

When changing the number of echoes in the SE experiment, also the time span was varied due to fixed echo spacing. This led to a heavier weighting of the slow pool and thus a larger observed T_2 value (Fig. 1b). As expected from the previous data, shorter echo spacing results in lower observed T_2 values.

The DESPOT2 outcome did not give a significant difference when changing TR from 3.25 ms to 10 ms (Fig. 2a and b). In the same results it was seen that the outcome of this method highly depends on the used flip angle combination. Also for the flip angle combination at which the optimal T_2 precision should be achieved (15° and 55°) a severe underestimation in T_2 compared to the SE results is observed (Fig. 2a and b). Another combination of flip angles (20° and 80°) (4) also resulted in underestimation of T_2 .

When investigating the influence of the fractional pool size, F , and the exchange rate, k , it is seen that the SE T_2 depends on these parameters (Fig. 2c). The DESPOT2 observation of T_2 also depends on these parameters, however, in a different manner (Fig. 2c and d). For the single pool situation ($F = 0$), SE results in the single input T_2 value while DESPOT2 underestimates T_2 slightly by 6.5 ms within the gray matter simulations (5% underestimation of T_2 compared to the SE observation; Fig. 2e and f). However, whenever a two compartment situation exists, an increased underestimation of T_2 is obtained by the DESPOT2 approach com-

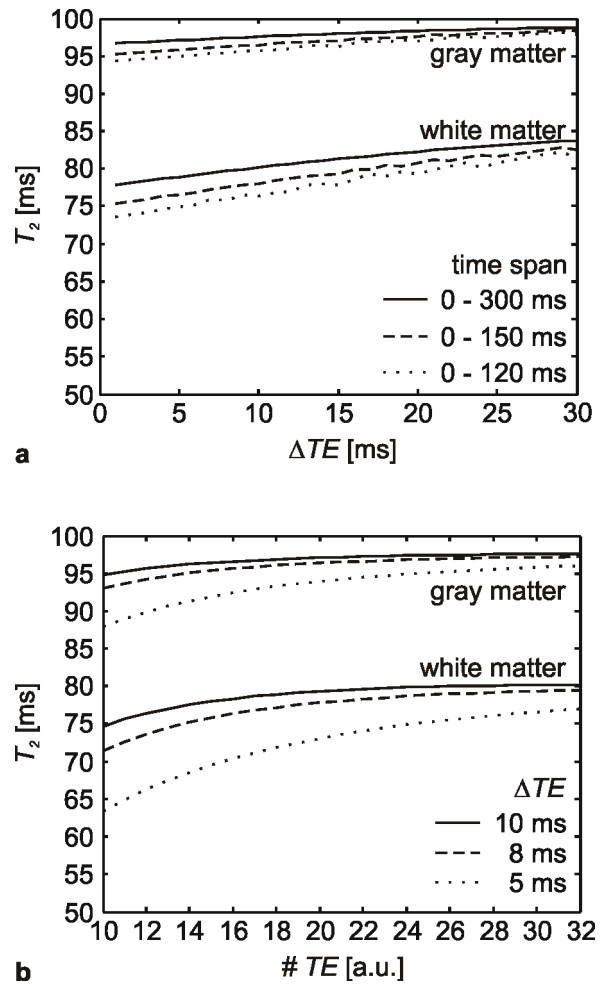


Figure 1. Simulation results of the spin echo sequence for tissue parameters as given in Table 1. The observed T_2 is given as a function of the echo spacing (a) and as a function of the number of echoes (b). The echo spacing in (a) is distributed over three time spans (0-300, 0-150, and 0-120 ms). With variation of the number of echoes, the time span covered by the echoes varies. The number of echoes is changed for $TE = 5, 8, 10$ ms (b), results only shown for time spans larger than the observed T_2 .

pared to the SE approach. The observed difference depends on the fraction and exchange rate (Fig. 2e and f).

Measurements

Spin echo experiments show identical results as the simulations (Fig. 3). Again only very limited change in T_2 could be observed due to a change in echo spacing. Shorter time span on the other hand, has a larger influence when approaching the lower limit in time span (time span = T_2).

The DESPOT2 calculations on the measurement data showed approximately identical T_2 values when measuring a single pool system (i.e., phantoms, Fig. 3a-c). Like in the simulations, a slight underestimation of T_2 by approximately 5% is observed between the SE and DESPOT2 ($\alpha_{1,2} = 15^\circ, 55^\circ$) T_2 observations. When measuring brain tis-

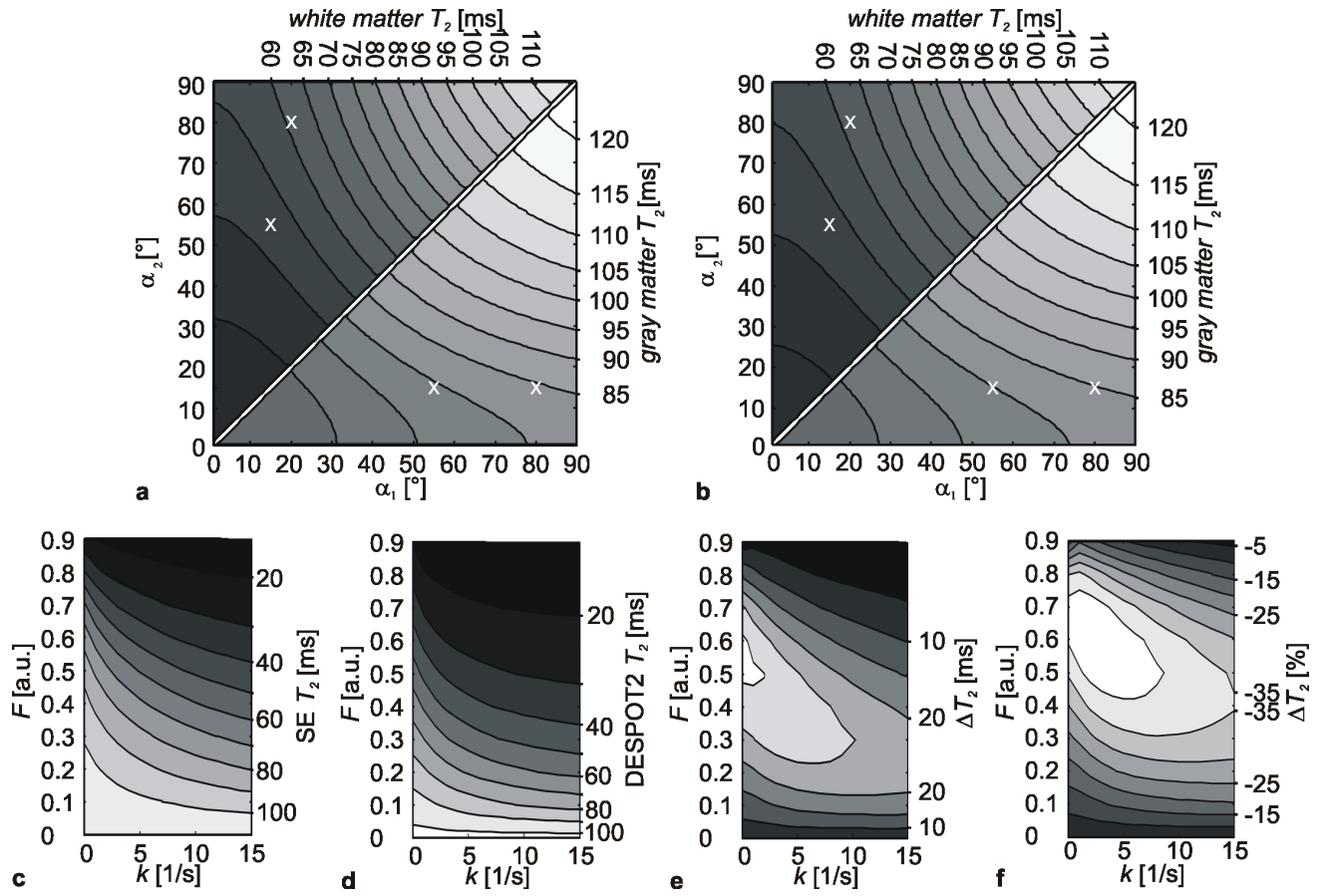


Figure 2. Results of the DESPOT2 simulations (a and b) for gray and white matter (bottom right and top left, respectively) as a function of the flip angles for $TR = 3.25$ ms (a) and $TR = 10$ ms (b). DESPOT2 flip angles used in literature ($15^\circ/55^\circ$ (3,19,21); $20^\circ/80^\circ$ (4)) are indicated by x-marks. SE based and DESPOT2 T_2 observation a function of the exchange rate k and the fast pool fraction F (c and d). Deviation of the DESPOT2 T_2 (d) from the SE T_2 (c) as a function of k and F expressed in ms (e) and expressed as a percentage of the SE T_2 (f). The parameters of the simulated tissue are given in Table 1.

sue, the DESPOT2 approach resulted in lower T_2 values (gray matter $T_2 = 62$ ms, and 60 ms; white matter $T_2 = 47$ ms and 44 ms; $15^\circ/55^\circ$ or $20^\circ/80^\circ$ bSSFP flip angle combination, respectively) as the SE approach (10 ms echo spacing, 32 echoes: gray matter $T_2 = 73$ ms; white matter $T_2 = 63$ ms). This is also in accordance to the observations in the simulation data. To prove the assumption of on-resonance in the simulations was also valid for the measurements, a B_0 map of the measurements was also provided. B_0 deviations are very limited (Fig. 3a and d) and it could therefore be considered that the data was acquired at on-resonance.

Table 2. Mean relaxation times and standard deviation derived from the simulations and measurements of gray and white matter. Simulation tissue characteristic parameters are given in Table 1.

TE time span	gray matter		white matter	
	simulation	measurement	simulation	measurement
0-120 ms	96.4 ms \pm 1.2 ms	71.6 ms \pm 1.0 ms	78.2 ms \pm 2.6 ms	60.4 ms \pm 0.8 ms
0-150 ms	97.0 ms \pm 1.0 ms	72.9 ms \pm 0.6 ms	79.4 ms \pm 2.3 ms	62.8 ms \pm 0.9 ms
0-300 ms	97.9 ms \pm 0.7 ms	72.4 ms \pm 0.1 ms	81.2 ms \pm 1.8 ms	66.1 ms \pm 0.5 ms

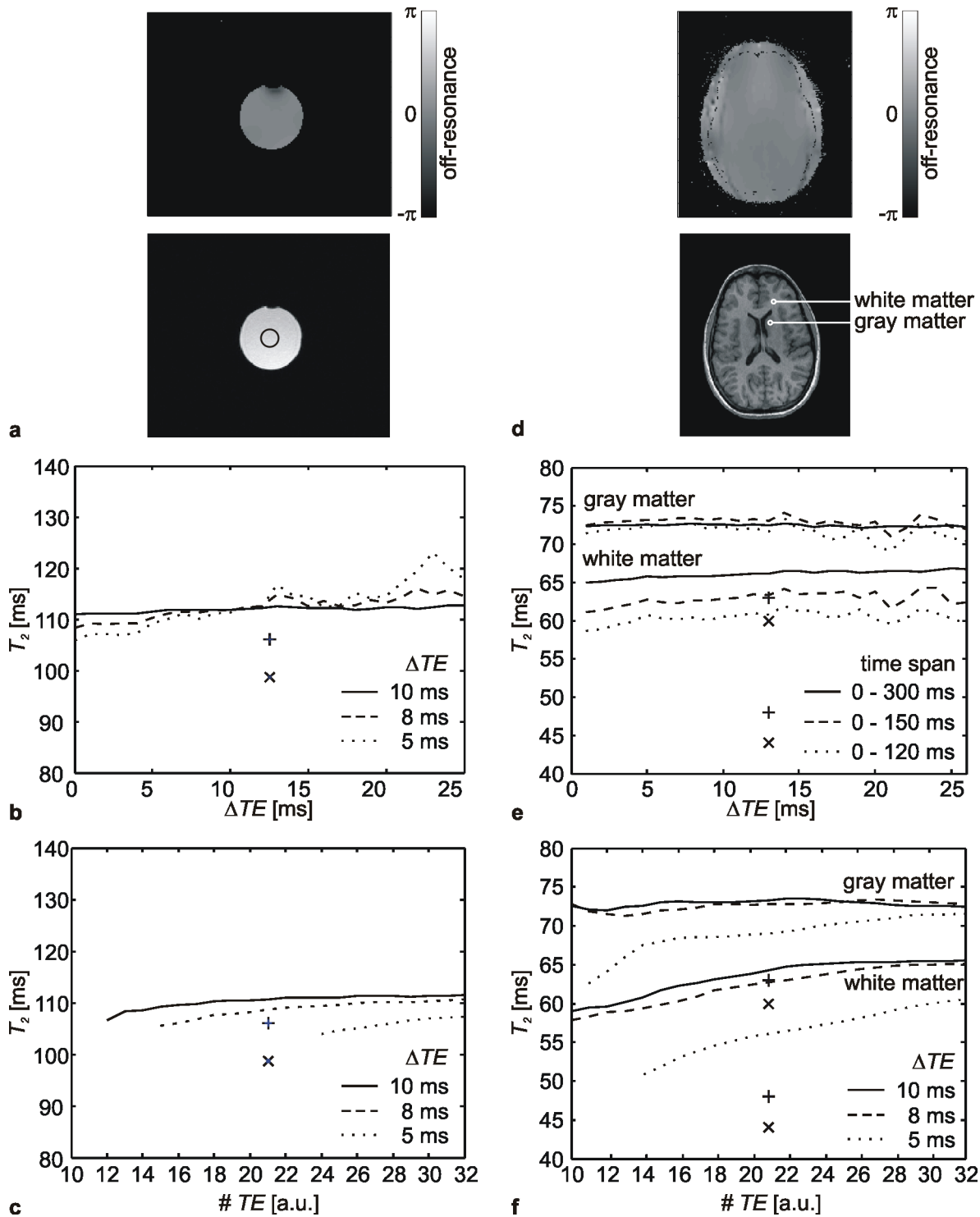


Figure 3. Measurement results for the 1 mM Gadolinium in water spherical phantom (a – c) and gray and white matter regions in human brain (d - f). At the top of (a) and (d), the B_0 map is showing the on/off-resonance of the measurements. Regions of interest are indicated in the 15° GRE images (bottom of a and d; only left side ROIs are indicated in the brain, although both sides were measured and averaged). Spin echo T_2 calculations are given as a function of the echo spacing (b and e), and as a function of the number of echoes included for the fit (c and f) for time spans $\geq T_2$. The T_2 values obtained by the DESPOT2 method are given as a + ($\alpha_{1,2} = 20^\circ, 80^\circ$) and x ($\alpha_{1,2} = 15^\circ, 55^\circ$).

DISCUSSION AND CONCLUSION

The influence of echo spacing on the observed T_2 value with the SE approach has shown to be insignificant when observing a coupled two compartment probe. A larger pools size increases this influence when k is constant (e.g. white matter vs. gray matter). However, for both gray and white matter, the effect of the echo spacing could still be considered negligible since the standard deviation over the investigated range did not exceed 4% of the mean observed T_2 . By increasing ΔTE , the $\#TE$ in a time span is reduced. This also did not significantly influence the outcome (also a standard deviation of less than 4% of the mean observed T_2). On the other hand, the sampled time span and the number of sampling points have shown of importance when going beyond the lower limit of time span (i.e., time spans shorter than the observed T_2), when observing a coupled two compartment probe. The commonly used multi echo spin echo setup with 10 ms echo spacing and 32 echoes (8,21) covers the time span 10-320 ms, far away from the lower limit in brain tissue (T_2 of brain tissue is typically below 100 ms).

For the same simulated coupled two compartment probes, it is proven that the TR of bSSFP has no significant influence on the outcome of the DESPOT2 method. The choice of flip angles has a larger influence on the outcome of this method. Although the choice of flip angles could change the outcome significantly, simulations did not show any result of the DESPOT2 method to be identical to that of the SE approach. Underestimation of T_2 was always achieved by the DESPOT2 method compared to the SE method. Variation in the pool fraction and the exchange rate between the compartments has shown that the two methods (SE and DESPOT2) give approximately identical T_2 values for a single compartment probe. The DESPOT2 method starts to largely underestimate the T_2 value (compared to the SE observed T_2 value), as soon as a second compartment is present.

The SE measurement results have proven the simulation results to be valid: also for in vivo measurement of brain tissue, the echo spacing does not influence the outcome of the method, the time span over which the data is acquired does, once going towards the time span = T_2 limit.

It was proven that the measurements were taken at on-resonance by means of the B_0 map; the

RF pulse duration was set long enough to avoid MT effect; the actual flip angle was taken for the DESPOT1 and DESPOT2 calculations; and finite pulse effects were corrected for within the DESPOT2 T_2 calculation. Therefore, the experiments were conform the assumptions made in the simulations and the results could be compared. As expected from the simulation data, the observation by the DESPOT2 method with typical flip angle choices underestimated T_2 compared to the typical SE approach: in gray matter, the underestimation was 11-13 ms (15-18%); in white matter a 16-19 ms (26-30%) underestimation was found.

The choice of echo spacing and time span over which the echoes are distributed within a SE experiment with mono-exponential T_2 fit affect the observed T_2 of a coupled two compartment probe only very little. Within the DESPOT2 approach, the TR choice does not affect the outcome; however, the choice of flip angles does and should therefore be carefully chosen. Nevertheless will the DESPOT2 approach always underestimate T_2 compared to the outcome of the standard SE approach. Although the SE approach takes a longer acquisition time, it has proven to be less dependent on sequence parameter settings than the DESPOT2 approach. In the case where one only needs a rough and quick estimation of a single T_2 value of a multi T_2 probe, the DESPOT2 approach is the favorable method of the two tested methods in this work. However, when a more accurate and less parameter setting sensitive T_2 quantification is desired, one needs limited but sufficient time and the SE approach with mono-exponential T_2 fit is in this case preferred.

ACKNOWLEDGEMENTS

This research was supported by the grants: SNF 325230-118377 and NCCR CO-ME.

REFERENCES

1. Wolff SD, Balaban RS. Magnetization transfer contrast (MTC) and tissue water proton relaxation in vivo. *Magn Reson Med* 1989;10(1):135-144.
2. Gelman N, Gorell JM, Barker PB, Savage RM, Spickler EM, Windham JP, Knight RA. MR imaging of human brain at 3.0 T: preliminary report on transverse relaxation rates and relation to estimated iron content. *Radiology* 1999;210(3):759-767.
3. Deoni SC, Peters TM, Rutt BK. High-resolution T1 and T2 mapping of the brain in a clinically acceptable time with DESPOT1 and DESPOT2. *Magn Reson Med* 2005;53(1):237-241.
4. Deoni SC, Rutt BK, Peters TM. Rapid combined T1 and T2 mapping using gradient recalled acquisition in the steady state. *Magn Reson Med* 2003;49(3):515-526.
5. Bartzokis G, Sultzer D, Cummings J, Holt LE, Hance DB, Henderson VW, Mintz J. In vivo evaluation of brain iron in Alzheimer disease using magnetic resonance imaging. *Arch Gen Psychiatry* 2000;57(1):47-53.
6. Pitkänen A, Laakso M, Kälviäinen R, Partanen K, Vainio P, Lehtovirta M, Riekkinen P, Soininen H. Severity of hippocampal atrophy correlates with the prolongation of MRI T2 relaxation time in temporal lobe epilepsy but not in Alzheimer's disease. *Neurology* 1996;46(6):1724-1730.
7. Williamson P, Pelz D, Merskey H, Morrison S, Karlik S, Drost D, Carr T, Conlon P. Frontal, temporal, and striatal proton relaxation times in schizophrenic patients and normal comparison subjects. *Am J Psychiatry* 1992;149(4):549-551.
8. Larsson HB, Frederiksen J, Petersen J, Nordenbo A, Zeeberg I, Henriksen O, Olesen J. Assessment of demyelination, edema, and gliosis by in vivo determination of T1 and T2 in the brain of patients with acute attack of multiple sclerosis. *Magn Reson Med* 1989;11(3):337-348.
9. Sussman MS, Vidarsson L, Pauly JM, Cheng HL. A technique for rapid single-echo spin-echo T2 mapping. *Magn Reson Med*;64(2):536-545.
10. Pell GS, Briellmann RS, Waites AB, Abbott DF, Jackson GD. Voxel-based relaxometry: a new approach for analysis of T2 relaxometry changes in epilepsy. *Neuroimage* 2004;21(2):707-713.
11. Stanisiz GJ, Odrobina EE, Pun J, Escaravage M, Graham SJ, Bronskill MJ, Henkelman RM. T1, T2 relaxation and magnetization transfer in tissue at 3T. *Magn Reson Med* 2005;54(3):507-512.
12. Poon CS, Henkelman RM. Practical T2 quantitation for clinical applications. *J Magn Reson Imaging* 1992;2(5):541-553.
13. Stewart WA, MacKay AL, Whittall KP, Moore GR, Paty DW. Spin-spin relaxation in experimental allergic encephalomyelitis. Analysis of CPMG data using a non-linear least squares method and linear inverse theory. *Magn Reson Med* 1993;29(6):767-775.
14. Vasilescu V, Katona E, Simplaceanu V, Demco D. Water compartments in the myelinated nerve. III. Pulsed NMR results. *Experientia* 1978;34(11):1443-1444.
15. Menon RS, Allen PS. Application of continuous relaxation time distributions to the fitting of data from model systems and excised tissue. *Magn Reson Med* 1991;20(2):214-227.
16. Lenz C, Klarhofer M, Scheffler K. Limitations of rapid myelin water quantification using 3D bSSFP. *MAGMA*;23(3):139-151.
17. Deoni SC, Rutt BK, Arun T, Pierpaoli C, Jones DK. Gleaning multicomponent T1 and T2 information from steady-state imaging data. *Magn Reson Med* 2008;60(6):1372-1387.
18. Bieri O, Scheffler K. On the origin of apparent low tissue signals in balanced SSFP. *Magn Reson Med* 2006;56(5):1067-1074.
19. Crooijmans HJA, Gloor M, Bieri O, Scheffler K. Influence of MT effects on T2 quantification with 3D balanced steady-state free precession imaging. 2010.
20. Bieri O, Scheffler K. SSFP signal with finite RF pulses. *Magn Reson Med* 2009;62(5):1232-1241.
21. Crooijmans HJA, Scheffler K, Bieri O. Finite RF pulse Correction on DESPOT2. *Magn Reson Med* 2010.
22. Bloch F. Nuclear induction. *Phys Rev* 1946;70:460-474.

5

Summary and Outlook

SUMMARY

The aim of this thesis was to test the capabilities of the DESPOT2 method to become the new principle technique for (volumetric) T_2 quantification of brain tissue. Up to now, the spin echo approach for T_2 quantification is considered the principle technique. The spin echo approach was therefore taken as a reference method throughout the thesis. To become the new principle method, the DESPOT2 method has to result in identical observation of T_2 as the present principle method. The tissue with most mechanisms affecting the observation by DESPOT2 is brain tissue. Brain tissue is therefore used as the ultimate test for comparison of the two methods after testing on aqueous phantoms, which were the simplest models. To investigate the above, the following questions were posed and the corresponding answers found and worked out in this thesis:

Chapter 2: *Does the magnetization transfer effect affect the outcome of the DESPOT2 method, and if so, how to avoid this?*

Numerical simulations were built, based on an underlying two pool model. The amount of MT effect within the obtained signal could be modified by adapting the duration of the RF excitation pulse: the longer the pulse, the less MT effect (1,2). Thereby, the MT free situation could be created, restoring the single pool model on which the DESPOT2 method is based. For simulations with short RF excitation pulses, the MT effect is increased with severely reduced observed T_2 as a result. Measurements on a healthy volunteer have proven the results of the simulation; however, additional underestimation is observed when shortening the pulse duration. Also within the phantom and CSF measurements, the observed T_2 value decreased by decreased duration of the RF excitation pulse. CSF and the phantom are single pool situations and it is thereby excluded that the underestimation is due to MT. The observed change in T_2 for phantom and CSF described the difference observed between simulations and measurements for gray and white matter. Nevertheless, both simulations and experiments have proven the influence of MT to be severe, directing towards the use of elongated RF excitation pulses to avoid the observed T_2 to be influenced by MT.

Chapter 3: *How can one avoid the finite pulse effect to influence the DESPOT2 calculation when using*

elongated RF excitation pulses?

Elongated RF excitation pulses within the bSSFP sequence make the obtained sequence prone to finite pulse effects (3). Short pulses approaching instantaneous RF pulses are to be avoided in order to avoid MT effects as shown in chapter 2 and the resulting finite pulse effect has to be taken into account. The correction for finite pulse effects as published in (3) was incorporated into the DESPOT2 equation to correct for the finite pulse effect within the calculation of T_2 . By means of a single pool Bloch simulation with finite RF pulse excitation, the incorporated correction was tested and proven to be effective in removing the finite pulse effect dependency from the DESPOT2 T_2 observation. Single pool Bloch simulations were used since they do not contain MT. By means of a two pool Bloch simulation, both MT and finite pulse effect were investigated, and it was determined that the finite pulse effect is dominant over the MT effect for $T_{RF}/TR > 0.15$. Measurements have proven the incorporated finite pulse correction to effectively remove the finite pulse effect from the T_2 observation, as predicted by the simulations. The observed additional deviation in T_2 as seen in chapter 2 could be explained by the finite pulse effect and now also be corrected for. Thus, MT effect can be avoided by elongation of the RF excitation pulses (chapter 2) and the dependency on finite pulse effects can be removed by the incorporation of the finite pulse effect correction in the DESPOT2 calculation (chapter 3).

Chapter 4: *How does the complex consistency of brain tissue, consisting of coupled pools of protons (e.g., myelin water – free water), affect the outcome of the DESPOT2 method, and how does it affect the spin echo approach (i.e., does the obtained T_2 depend on the choice of echo spacing)?*

Although, as explained in chapter 2 and 3, it is possible to avoid MT effect and correct for the finite pulse effect within the DESPOT2 T_2 observation, the method still overlooks the microscopic complexity of brain tissue (4-10). Even while brain tissue consists of multiple (coupled) compartments (4-10), it is often analyzed as a single T_2 probe (11-21). This is also the case in DESPOT2 and mono-exponential fit through SE data. Therefore, two pool simulations were used to investigate the influence of a coupled two pool system on the observation of a single T_2 by SE and DESPOT2. Within the SE method, several constant echo spacing settings were used to investigate the influence of this

on the outcome. It was shown by simulations and proven by measurements that the choice of echo spacing does not affect the observed T_2 ; however, the time span over which the sampling points were distributed shows to be of influence, when not chosen to be larger than the observed T_2 . The DESPOT2 method, on the other hand, has shown large dependency on its flip angle choice. The flip angle combinations used in literature ($15^\circ/55^\circ$ (13) and $20^\circ/80^\circ$ (14)) underestimate T_2 compared to the SE observation. The difference between the two methods depends on the pool fractions. While going towards the limit of a single pool situation, both methods result in similar T_2 observation. The exchange rate has less influence on the observed T_2 difference. It could thus be concluded that the SE observation of T_2 did not depend on the echo spacing, and that the DESPOT2 method underestimated T_2 independent of the used flip ($\alpha \ll 90^\circ$).

Overall, it is thus proven that MT influences the outcome of the DESPOT2 method, but can be avoided by the use of long RF excitation pulses. This on its turn introduces the finite pulse effect, which can be corrected for by a simple modification of the T_2 calculation as used in the DESPOT2 method. Although the effect of these two mechanisms can be eliminated, the effect of the complex microscopic structure of brain tissue still affects the outcome leading to an underestimation of T_2 by the DESPOT2 method compared to the SE observation. So far, the DESPOT2 method could become the principle method as long as the microscopic structure of the investigated tissue is not too complex, i.e., the tissue should not consist of a coupled multi compartment system. For example, cartilage measurements suffer from MT effect, but it has no coupled multi compartment microstructure such as is present in brain tissue. In those cases, the DESPOT2 method will result in identical observation of T_2 as SE, as long as elongated RF excitation pulses are used and the finite pulse effect is corrected for.

OUTLOOK

Future work will focus on the DESPOT1 method. This method is commonly used in combination with the DESPOT2 method to obtain prior knowledge of T_1 . Since the estimation of T_1 might fulfill a critical role in the precision of the T_2 estimate of DESPOT2, further investigation to the T_1 observation by DESPOT1 is welcome. Similar to the work presented in this thesis, investigation to the **finite pulse effect on the T_1 observation** should be performed and a possible correction implemented in the T_1 calculation of DESPOT1. It is already known that the finite pulse effect affects the obtained signal in an SPGR sequence (22), which is the basis of the DESPOT1 method. Afterwards, **flip angle choices** for DESPOT1 have to be analyzed further, and it has to be found if the DESPOT1 method depends on the **pool fractions** and **exchange rates** as the DESPOT2 method does. The DESPOT1 method should be compared to the principle method in T_1 quantification, inversion recovery spin echo. Again, a single T_1 observation is performed on the complex tissue of the brain, like the single T_2 observation of DESPOT2. More information and understanding of how this affects the outcome of the DESPOT1 method is needed to fully understand why the DESPOT2 method generally underestimates T_2 as compared to the principle method, SE.

Clinical applications of the DESPOT1 and DESPOT2 method have to be further explored. Although the clinical application of T_2 quantification on brain diseases has proven to be useful, this thesis has shown the drawback of brain imaging with these methods due to overlooking the complexity of the coupled two pool behavior of brain tissue. Other clinically interesting and relevant areas have to be explored. **Cartilage** could be a very interesting area of investigation. For example, cartilage in the knee joint, on the inside of the patella, is known to be prone to magnetization transfer, which in this thesis is proven to be a minor problem and can be overcome. Next to this, the interesting part of the cartilage of the patella is its dual layer behavior. The part close to the bone has different properties than its surface layer. The cartilage layer is not very thick, and high resolution is desired. The DESPOT1 and DESPOT2 methods offer a high resolution ($< 1 \text{ mm}^3$ isotropic) volumetric quantification of T_1 and T_2 within approximately 20 minutes (13). With the implemented finite pulse correction and the use of long RF excitation pulses, T_1 and T_2 can be ob-

served without any influence of MT. Clinically interesting would be to investigate T_1 and T_2 changes due to damaged cartilage. Besides the cartilage of the patella, also the cartilage layer of the knee joint itself might be of interest. Possible early detection of damaged cartilage might offer the opportunity of non invasive treatment rather than the need for knee prosthesis.

Another field of interest for the application of volumetric T_1 and T_2 quantification is in the field of **forensic medicine**. This field allows the acquisition of e.g. cardiac images without the motion and flow present in the living. The use of quantitative imaging might give information not only on the cause of death (e.g. myocardial infarct, pulmonary fat embolisms), but it might possibly give additional information on the time passed since death (e.g. quantification of rigor mortis). Besides the quantification of T_1 and T_2 , quantification of other parameters such as diffusion, MT and fat-water separation will be investigated to find its use in forensic medicine. Since forensic medicine is a relatively new field of application of MR, there are many opportunities for new applications. One great advantage is the absence of motion and flow, leading to the possibility of applying methods that cannot be applied on living humans due to, for example, desire for extremely long breath holds, occurrence of flow or motion artifacts. Knowledge obtained from this field might provide new insights that can ease an autopsy (e.g. it might indicate how to slice the heart in order to optimally show the size of a myocardial infarction) or omit the need of invasive autopsy and by means of MR scanning prove a certain cause of death. Beyond the field of forensic medicine, clinical medicine might benefit from the knowledge gained here due to the options of elongated scans which are not possible to perform on patients. Therefore, the research performed in the field of forensic medicine might provide useful information that can be correlated to other, faster, scanning methods with clinically acceptable acquisition times, and become clinically relevant.

REFERENCES

1. Bieri O, Scheffler K. Optimized balanced steady-state free precession magnetization transfer imaging. *Magn Reson Med* 2007;58(3):511-518.
2. Gloor M, Scheffler K, Bieri O. Quantitative magnetization transfer imaging using balanced SSFP. *Magn Reson Med* 2008;60(3):691-700.
3. Bieri O, Scheffler K. SSFP signal with finite RF pulses. *Magn Reson Med* 2009;62(5):1232-1241.
4. Lenz C, Klarhofer M, Scheffler K. Limitations of rapid myelin water quantification using 3D bSSFP. *MAGMA*;23(3):139-151.
5. Deoni SC, Rutt BK, Arun T, Pierpaoli C, Jones DK. Gleaning multicomponent T1 and T2 information from steady-state imaging data. *Magn Reson Med* 2008;60(6):1372-1387.
6. Deoni SC, Rutt BK, Jones DK. Investigating exchange and multicomponent relaxation in fully-balanced steady-state free precession imaging. *J Magn Reson Imaging* 2008;27(6):1421-1429.
7. Laule C, Leung E, Lis DK, Traboulsee AL, Paty DW, MacKay AL, Moore GR. Myelin water imaging in multiple sclerosis: quantitative correlations with histopathology. *Mult Scler* 2006;12(6):747-753.
8. MacKay A, Laule C, Vavasour I, Bjarnason T, Kolind S, Madler B. Insights into brain microstructure from the T2 distribution. *Magn Reson Imaging* 2006;24(4):515-525.
9. MacKay A, Whittall K, Adler J, Li D, Paty D, Graeb D. In vivo visualization of myelin water in brain by magnetic resonance. *Magn Reson Med* 1994;31(6):673-677.
10. Whittall KP, MacKay AL, Graeb DA, Nugent RA, Li DK, Paty DW. In vivo measurement of T2 distributions and water contents in normal human brain. *Magn Reson Med* 1997;37(1):34-43.
11. Stanisz GJ, Odrobina EE, Pun J, Escaravage M, Graham SJ, Bronskill MJ, Henkelman RM. T1, T2 relaxation and magnetization transfer in tissue at 3T. *Magn Reson Med* 2005;54(3):507-512.
12. Gelman N, Gorell JM, Barker PB, Savage RM, Spickler EM, Windham JP, Knight RA. MR imaging of human brain at 3.0 T: preliminary report on transverse relaxation rates and relation to estimated iron content. *Radiology* 1999;210(3):759-767.
13. Deoni SC, Peters TM, Rutt BK. High-resolution T1 and T2 mapping of the brain in a clinically acceptable time with DESPOT1 and DESPOT2. *Magn Reson Med* 2005;53(1):237-241.
14. Deoni SC, Rutt BK, Peters TM. Rapid combined T1 and T2 mapping using gradient recalled acquisition in the steady state. *Magn Reson Med* 2003;49(3):515-526.
15. Bartzokis G, Sultzer D, Cummings J, Holt LE, Hance DB, Henderson VW, Mintz J. In vivo evaluation of brain iron in Alzheimer disease using magnetic resonance imaging. *Arch Gen Psychiatry* 2000;57(1):47-53.
16. Pitkanen A, Laakso M, Kalviainen R, Partanen K, Vainio P, Lehtovirta M, Riekkinen P, Soininen H. Severity of hippocampal atrophy correlates with the prolongation of MRI T2 relaxation time in temporal lobe epilepsy but not in Alzheimer's disease. *Neurology* 1996;46(6):1724-1730.
17. Williamson P, Pelz D, Merskey H, Morrison S, Karlik S, Drost D, Carr T, Conlon P. Frontal, temporal, and striatal proton relaxation times in schizophrenic patients and normal comparison subjects. *Am J Psychiatry* 1992;149(4):549-551.
18. Larsson HB, Frederiksen J, Petersen J, Nordenbo A, Zeeberg I, Henriksen O, Olesen J. Assessment of demyelination, edema, and gliosis by in vivo determination of T1 and T2 in the brain of patients with acute attack of multiple sclerosis. *Magn Reson Med* 1989;11(3):337-348.
19. Sussman MS, Vidarsson L, Pauly JM, Cheng HL. A technique for rapid single-echo spin-echo T2 mapping. *Magn Reson Med*;64(2):536-545.
20. Pell GS, Briellmann RS, Waites AB, Abbott DF, Jackson GD. Voxel-based relaxometry: a new approach for analysis of T2 relaxometry changes in epilepsy. *Neuroimage* 2004;21(2):707-713.

21. Poon CS, Henkelman RM. Practical T2 quantitation for clinical applications. *J Magn Reson Imaging* 1992;2(5):541-553.
22. Boulant N. T1 and T2 effects during radio-frequency pulses in spoiled gradient echo sequences. *J Magn Reson* 2009;197(2):213-218.

6

Acknowledgement

A PhD thesis is an original piece of work, written by a single author. However, the author cannot succeed the writing of this work without the help of many. While writing, I finally arrived at the part where I can acknowledge the people that helped me to fulfill this task over the last years. Help consisted of work related and less work related things. Both of them are very important. Since this is a personal note to the people concerned, I will address them by the names I use in day to day life.

First of all, I thank my supervisors Klaus, Oli, and Oliver, for their time spent with me for scientific discussions, brainstorming on ideas, and their critical notes to my work, helping me to improve the quality of my research. Their enthusiasm, knowledge and assistance were of great help.

Second, I would like to thank all my colleagues, for the joy we had every day, making it a pleasure to get to work, day in day out, even when my work was doing all possible to work against me. Especially I would like to thank 'shorty' for letting me bump her on de head at least once a day, making fun over a coffee break, and many more fun things we did in the time she was my office-neighbour. Francesco, thank you for your help, always and every time I had a (stupid) question, you patiently helped me. Julia, thank you for 'volunteering' as a paper ball target whenever Oli and I had our moment of fun and needed to throw paper balls at you.

However, although the above is very valuable, I would not have reached the point of starting a PhD thesis in Basel without the great basis that is given to me at home. My parents and grandparents always supported me in my ideas, helping me to chase my dreams. As my granddad used to say, whenever I came to him with a story in the days he was still among us: 'volhouden jongen, volhouden' ('keep going boy, keep going'), while making his hand into a fist to give some extra power to the words and extra motivation to me. This has always been in my memory when times were tough. From my other granddad I have also had the opportunity to learn a lot, and I still do every time I talk to him. From him I have learned to chase dreams, no matter how difficult the way is to reach your goal, never give up and keep trying. Never stop believing in your capabilities, no matter what other people say. Always give it this one more try! What I will never forget is what he always says when times are tough: 'onkruid vergaat niet!' Both of my grandfathers have never hidden the fact or missed an opportunity to let me know they could not be this success-

ful without the help of their wives, my grandmothers. In other words, one cannot succeed on his own, one needs help.

While writing my thesis, my best friend from the Netherlands, who I know already for many years, came over to Basel. She stayed here while I was in full working mode, no time to think of anything else than my thesis. Chasing my dream to finish it. She helped my dear Sarah to withstand my total ignorance of the world around me during these days. I would like to thank her for being such a good friend over all the years.

Two friends that I should not forget to mention are Sander and Nancy. Sander is the friend that over the years was one of the most regular visitors and a good help whenever needing someone to talk to. Although we do not see each other as regular as in the time we both lived in Eindhoven, the friendship did not suffer. Nancy, although traveling around the world for one year, is always there for me when I need her, no matter where on this planet she will be. It is great to have a friend like her, appreciating every little moment we can spend together, never complaining about the long times we sometimes do not find time. Thank you both!

Last but definitely not least I have to thank Sarah, she dared to start this adventure with me from the beginning. She joined me when I wanted to move abroad. She has always been there for me, even in times when life was not only full of joy and happiness. Especially for those times, thank you very much for being there and never leaving my side! Dankjewel schat, voor alles!

I look forward to the many more pleasant and joyful moments we plan to have together. Above all, the simple joy of being together.

For all of you that might think they are forgotten:

The space is simply too limited to write a personal note to every single one of you, and although perhaps not mentioned by (nick)name, you are not forgotten: Thank you all for your support, help and joy!

7

List Of Publications and Curriculum Vitae

LIST OF PUBLICATIONS

Journal Publications

G. Schulz, **H.J.A. Crooijmans**, M. Germann, K. Scheffler, M. Müller-Gerbl, A. Morel and B. Müller. Three-dimensional strain fields in human brain resulting from formalin fixation. *J Neurosci Meth.* Submitted 2011

A. Papadimitropoulos, A. Scherberich, S. Gueven, N. Theilgaard, **H.J.A. Crooijmans**, F. Santini, K. Scheffler, A. Zallone and I. Martin. A 3D in vitro bone organ model using human progenitor cells. *Eur Cells Mater.* 21:445-458, 2011

H.J.A. Crooijmans, K. Scheffler and O. Bieri. Finite RF pulse correction on DESPOT2. *Magn Reson Med*, 65(3):858-862, 2010

H.J.A. Crooijmans, M. Gloor, O. Bieri and K. Scheffler. Influence of MT effects on T_2 quantification with 3D balanced steady-state free precession imaging. *Magn Reson Med.* 65(1):195-201, 2010

H.J.A. Crooijmans, A.M.R.P. Laumen, C. van Pul and J.B.A. van Mourik, A new digital preoperative planning method for total hip arthroplasty. *Clin Orthop Relat Res.* 467(4):909-916, 2009

Conference Abstracts

H.J.A. Crooijmans, T. Ruder, S. mathier, M.J. Thali, K. Scheffler and O. Bieri. Diffusion mapping in the post mortem porcine and human heart after possible myocardial infarct. *Proceedings of the 28th annual scientific meeting of ESMRMB*, Leipzig, Germany, October 6-8 2011

H.J.A. Crooijmans, T. Ruder, S. mathier, M.J. Thali, K. Scheffler and O. Bieri. Cardiac MTR mapping in forensic medicine. *Proceedings of the 28th annual scientific meeting of ESMRMB*, Leipzig, Germany, October 6-8 2011

H.J.A. Crooijmans, M. Gloor, K. Scheffler and O. Bieri. Single pool assumption in SE and DESPOT2 T2 quantifications on multi-T2 probes. *Proceedings of the 28th annual scientific meeting of ESMRMB*, Leipzig, Germany, October 6-8 2011

N. Hainc, **H.J.A. Crooijmans** and K. Scheffler. Imaging of microarchitecture in the proximal femur at 1.5T and 3.0T. *Proceedings of the 28th annual scientific meeting of ESMRMB*, Leipzig, Germany, October 6-8 2011

H.J.A. Crooijmans, F. Santini, P.C. Cattin, O.M. Weber, and K. Scheffler. Quantification of blood flowing through the tricuspid valves throughout the cardiac cycle. *Proceedings of the 28th annual scientific meeting of ESMRMB*, Leipzig, Germany, October 6-8 2011

H.J.A. Crooijmans, K. Scheffler and O. Bieri. The influence of finite long pulse correction on DESPOT2. *Proceedings of the ISMRM-ESMRMB Joint Annual Meeting*, Stockholm, Sweden, May 1-7 2010

H.J.A. Crooijmans, P.C. Cattin, O.M. Weber and K. Scheffler. Cardiac valve prediction in CINE-bSSFP images using SURF. *Proceedings of the ISMRM-ESMRMB Joint Annual Meeting*, Stockholm, Sweden, May 1-7 2010

H.J.A. Crooijmans, A. Papadimitropoulos, F. Santini, I. Martin and K. Scheffler. A non-invasive Magnetic Resonance Imaging (MRI) based method assessing the extent of bone remodeling in an in-vitro bone organ model. *Proceedings of the 26th annual scientific meeting of ESMRMB*, Antalya, Turkey, October 1-3 2009

H.J.A. Crooijmans, G. Schulz, M. Müller-Gerbl and K. Scheffler. Postmortem MRI of human brain: T₁ and T₂ relaxation times during formaldehyde fixation, *Proceedings of the 26th annual scientific meeting of ESMRMB*, Antalya, Turkey, October 1-3 2009

H.J.A. Crooijmans, A. Papadimitropoulos, F. Santini, I. Marin and K. Scheffler. Assessing the extent of bone remodeling in an in vitro bone organ model by MRI, *Proceedings of the SSBE annual meeting*, Bern, Switzerland, August 27-28 2009

H.J.A. Crooijmans, K. Scheffler and O. Bieri. Effect of magnetization transfer on rapid T₂ estimation with phase-cycled variable nutation SSFP. *Proceedings of the 17th scientific meeting & exhibition of ISMRM*, Honolulu, USA, April 18-24 2009

H.J.A. Crooijmans, A. Papadimitropoulos, I. Martin, K. Scheffler, S. Riboldi and F. Santini. Non-invasive monitoring of collagen type I concentration in scaffolds through MRI. *Proceedings of the 25th annual meeting of ESMRMB*, Valencia, Spain, October 2-4 2008

H.J.A. Crooijmans and K. Scheffler. TR/T₂ dependency of variable flip angle T₁ measurements, a simulation, *Proceedings of the 25th annual meeting of ESMRMB*, Valencia, Spain, October 2-4 2008

H.J.A. Crooijmans, A. Papadimitropoulos, I. Marin, K. Scheffler, S. Riboldi and F. Santini. Magnetic resonance imaging for monitoring the growth of extracellular matrix on porous scaffolds. *Proceedings of the SSBE annual meeting*, Muttenz, Switzerland, September 4-5 2008

CURRICULUM VITAE

Personal Data

Surname	Crooijmans
Given names	Hendrikus Joseph Alphons
Date of birth	05/05/1982
Place of birth	Utrecht, the Netherlands

Education

Sep 2007 – June 2011

Ph.D. thesis, University of Basel. Supervisors: O. Bieri, Ph.D., O.W. Weber, Ph.D., prof. K. Scheffler, Ph.D.
Field: biophysics

Aug 2004 – May 2007

Master in BioMedical Engineering, Eindhoven University of Technology, Eindhoven, the Netherlands

Aug 2000 – Aug 2005

Bachelor in BioMedical Engineering, Eindhoven University of Technology, Eindhoven, the Netherlands

Aug 1994–Jun 2000

Atheneum, Dr. Knippenbergcollege, Helmond, the Netherlands (Dutch,English, physics, chemistry, mathematics, geography and biology). Diploma qualifying for university admittance (A-level).

